Check for updates

ADVANCED FUNCTIONAL MATERIALS
www.afm-journal.de

Macrophage Hitchhiking Nanoparticles for the Treatment of Myocardial Infarction: An In Vitro and In Vivo Study

Giulia Torrieri, Imran Iqbal, Flavia Fontana, Virpi Talman, Heidi Liljenbäck, Andriana Putri, Wail Nammas, Johan Rajander, Xiang Guo-Li, Philip S. Low, Tambet Teesalu, Anne Roivainen, Jouni Hirvonen, Heikki Ruskoaho, Vimalkumar Balasubramanian,* Antti Saraste,* and Hélder A. Santos**

Myocardial infarction (MI) is the leading cause of death worldwide. However, current therapies are unable to restore the function of the injured myocardium. Advanced approaches, such as stimulation of cardiomyocyte (CM) proliferation are promising, but suffer from poor pharmacokinetics and possible systemic adverse effects. Nanomedicines can be a solution to the above-mentioned drawbacks. However, targeting the cardiac tissue still represents a challenge. Herein, a MI-selective precision nanosystem is developed, that relies on the heart targeting properties of atrial natriuretic peptide (ANP) and lin-TT1 peptide-mediated hitchhiking on M2-like macrophages. The system based on pH-responsive putrescine-modified acetalated dextran (Putre-AcDEX) nanoparticles, shows biocompatibility with cultured cardiac cells, and ANP receptor-dependent interaction with CMs. Moreover, treatment with nanoparticles (NPs) loaded with two pleiotropic cellular self-renewal promoting compounds, CHIR99021 and SB203580, induces a 4-fold increase in bromodeoxyuridine (BrdU) incorporation in primary cardiomyocytes compared to control. In vivo studies confirm that M2-like macrophages targeting by lin-TT1 peptide enhances the heart targeting of ANP. In addition, NP administration does not alter the immunological profile of blood and spleen, showing the short-term safety of the developed system in vivo. Overall, the study results in the development of a peptide-guided precision nanosystem for delivery of therapeutic compounds to the infarcted heart.

1. Introduction

Myocardial infraction (MI) is the leading cause of death worldwide, accounting for approximately half of all cardiovascular deaths.[1] Obstruction of the arteries supplying blood to the cardiac tissue causes heart ischemia with irreversible massive death of cardiac cells and subsequent deposition of non-contractile tissue.[2,3] Pharmacological stimulation of cardiomyocyte (CM) proliferation is among the most appealing and promising approaches to tackle the loss of contracting cells.[3,4] Even though mammalian CMs retain the ability to proliferate only in the early postnatal life, treatment of adult CMs with miRNAs,[5–7] transcription factors,[8–11] small molecules[12] or combination of those,[12,13] has enabled their re-entry in cell cycle. Translation of such approaches is still hampered by poor pharmacokinetic profile of the compounds used to stimulate CMs proliferation, as well as by their potential systemic toxicity.[4]

Nanomedicines have brought great innovation in the medical field for the treatment of various diseases.[14,15] The ability to carry payloads specifically to target

G. Torrieri, F. Fontana, J. Hirvonen, H. A. Santos
Drug Research Program
Division of Pharmaceutical Chemistry and Technology
Faculty of Pharmacy
University of Helsinki
Helsinki FI-00140, Finland
E-mail: giulia.torrieri@helsinki.fi; h.a.santos@umcg.nl

I. Iqbal, H. Liljenbäck, A. Putri, W. Nammas, X. Guo-Li, A. Roivainen, A. Saraste
Turku PET Centre
University of Turku
Turku 20521, Finland
E-mail: antsaras@utu.fi

V. Talman, H. Ruskoaho
Drug Research Program
Division of Pharmacology and Pharmacotherapy
Faculty of Pharmacy
University of Helsinki
Helsinki FI-00140, Finland

H. Liljenbäck, A. Roivainen
Turku Center for Disease Modeling
University of Turku
Turku FI-20014, Finland

The ORCID identification number(s) for the author(s) of this article can be found under https://doi.org/10.1002/adfm.202303658

© 2023 The Authors. Advanced Functional Materials published by Wiley-VCH GmbH. This is an open access article under the terms of the Creative Commons Attribution License, which permits use, distribution and reproduction in any medium, provided the original work is properly cited.

DOI: 10.1002/adfm.202303658

sites, increasing the efficacy of treatments while reducing systemic adverse effects, can give a second life to many drugs and improve the performance of current available therapies.[14,15] Engineering nanocarriers to reach specific targets in our body is not a simple task and requires taking into account of different factors. Whereas the damaged cardiac tissue can potentially benefit from targeted delivery of novel nanotherapeutics, development of heart targeted nanodrugs remains challenging due to constant pumping of the heart, making it mechanically difficult to address,[16] and the lack of cell membrane markers exclusive to CMs, that could serve as targets for affinity ligands in vivo. Several approaches have been attempted in the past to achieve heart targeting from peptides[17,18] or antibody[19] targeting to possible cellular hitchhiking.[20]

J. Rajander
Accelerator Laboratory
Åbo Akademi University
Turku FI-20500, Finland

X. Guo-Li, A. Roivainen
InFLAMES Research Flagship Center
University of Turku
Turku Finland

P. S. Low
Department of Chemistry
Purdue University
West Lafayette, IN 47907-2084, USA

T. Teesalu
Laboratory of Cancer Biology
Institute of Biomedicine and Translational Medicine
Centre of Excellence for Translational Medicine
University of Tartu
Tartu 50411, Estonia

T. Teesalu
Cancer Research Center
Sanford-Burnham Medical Research Institute
La Jolla, California 92037, USA

A. Roivainen, A. Saraste
Turku PET Centre
Turku University Hospital
Turku 20521, Finland

V. Balasubramanian
Chemical and Pharmaceutical Development
Bayer Oy
Turku FI-20210, Finland
E-mail: vimalkumar.balasubramanian@bayer.com

A. Saraste
Heart Center
Turku University Hospital
Turku 20521, Finland

A. Saraste
Institute of Clinical Medicine
Turku University Hospital
Turku 20520, Finland

H. A. Santos
Department of Biomedical Engineering
University Medical Center Groningen
University of Groningen
A. Deusinglaan 1, AV Groningen 9713, The Netherlands

H. A. Santos
W.J. Kolff Institute for Biomedical Engineering and Materials Science
University Medical Center Groningen
University of Groningen
A. Deusinglaan 1, AV Groningen 9713, The Netherlands

Recently, we proposed a synergistic nanosystem that combines peptide targeting with cellular hitchhiking [21] with the aim to improve heart homing. The system consists of pH-responsive Putre-AcDEX nanoparticles (NPs), that are modified, through a branched polyethylene glycol (PEG), with ANP and p32-targeting linear TT1 (lin-TT1, aminoacid sequence: AKRGARSTA) peptide.[21] The pH-responsiveness of Putre-AcDEX is due to the presence of acetal groups in the AcDEX, which hydrolyze in the acidic subcellular compartment of the cells, promoting the intracellular delivery of two cellular self-renewal promoting compounds, CHIR99021 and SB203580.[21] The heart targeting properties of ANP have already been extensively investigated in past by our group,[17] while lin-TT1 is known for its homing to tumor macrophages and macrophages associated to atherosclerotic plaques.[22–24]

Considering that in MI inflammation has a key role in the outcome of the insult,[25,26] we have previously studied the interaction of our nanosystem with both M1– and M2–like macrophages to find out which subset is the most suitable to obtain the greater hitchhiking effect to the infarcted heart. It is known that immediately after a MI, neutrophils accumulate in the injured area to remove debris and dead cells, and further recruit monocytes, which then differentiate into inflammatory M1–type macrophage with the aim to "clean" the area and make space for the future scar.[25,26] The M1–like macrophage accumulation peaks ≈day 3 post-MI and it is followed by a remodeling phase characterized by the arrival of M2–like macrophages, which in turn, have a peak of accumulation ≈day 7 post-MI.[25,26] These M2–like macrophages secrete a series of cytokines, e.g. vascular endothelial growth factor (VEGF) and transforming growth factor (TGF)-β, which promote vascularization and fibrotic remodeling of the tissue, respectively.[25,26]

Our observation that Putre-AcDEX-PEG-TT1-ANP NPs showed a higher association-versus-uptake ratio with both human and murine M2–like macrophages led us to hypothesize that these cells can be targeted in vivo to maximize hitchhiking effect, and thus, improve the heart targeting properties of ANP.[21] Compared to current approaches, the hitchhiking effect-based targeting could result in a superior accumulation of carriers in the infarcted heart and increased therapeutic benefits. We hypothesize that the hitchhiking effect will lead to increased accumulation of NPs in the infarcted heart, due to interaction of lin-TT1 with p32 receptors on the surface of inflammatory cells. We assume that interaction with inflammatory cells will take place both in the circulation, resulting in macrophages giving a piggyback to the nanosystem to the infarcted heart, where they are recruited, and with the macrophages that are already accumulated in the site of injury. Once in the heart, the NPs will interact with ANP receptors on the surface of CMs and this will lead to internalization of the system.

The main aim of this work is to study the in vivo biodistribution of Putre-AcDEX-PEG-TT1-ANP NPs in a rat model of MI by investigating the accumulation of the system in the infarcted heart after 3 and 7 days post-MI, for the evaluation of the hitchhiking effect of either M1– and M2–like macrophages. Besides, we assess the in vitro biocompatibility and interaction of Putre-AcDEX NPs with cardiac cells of different origin (rat, mouse, and human). The delivery of the two cellular self-renewal promoting compounds, CHIR99021, and SB203580,[12] to cardiac cells and

© 2023 The Authors. Advanced Functional Materials published by Wiley-VCH GmbH

16163028, 0, Downloaded from https://onlinelibrary.wiley.com/doi/10.1002/adfm.202303658 by University of Turku, Wiley Online Library on [31/05/2023]. See the Terms and Conditions (https://onlinelibrary.wiley.com/terms-and-conditions) on Wiley Online Library for rules of use; OA articles are governed by the applicable Creative Commons License

16163028, 0, Downloaded from https://onlinelibrary.wiley.com/doi/10.1002/adfm.202303658 by University of Turku, Wiley Online Library on [31/05/2023]. See the Terms and Conditions (https://onlinelibrary.wiley.com/terms-and-conditions) on Wiley Online Library for rules of use; OA articles are governed by the applicable Creative Commons License

their effect on CMs proliferation is also investigated. Finally, the therapeutic potential of the nanosystem was assessed by studying the in vivo remodeling of the infarcted myocardium and the accumulation of inflammatory cells up to 90 days post-MI. Our study resulted in development of a peptide-guided nanosystem for delivery of therapeutic compounds to the infarcted heart for improved management of MI.

2. Results and Discussion

2.1. Nanoparticles Synthesis and Physicochemical Characterization

Putre-AcDEX NPs were obtained by using an oil-in-water (o/w) single emulsion technique, as previously described.[21] Surface modification steps were optimized to obtain NPs conjugated with both lin-TT1 and ANP, with small size and acceptable polydispersity index (PDI) values. Ethylenediaminetetraacetic acid (EDTA) was added during the coupling reaction between PEGylated NPs and TT1 to stabilize the thiol groups involved in the reaction between TT1 and the maleimide moieties of PEG.[27] Size, PDI, and zeta (ζ)-potential values obtained during each conjugation step are shown in Figure S1A (Supporting Information). The increase of NPs size after conjugations was modest and the PDI values showed a monodispersed NP's suspension. Surface charge values of the NPs (Figure S1A, Supporting Information), provided a tool to follow the conjugation steps. The ζ-potential values for bare Putre-AcDEX NPs were positive due to the presence of amine groups in putrescine. After PEGylation, the charge switched to negative values, due to deprotonated carboxylic groups of PEG and then exhibited an increase toward positive values after conjugation with ANP, which contains in its structure arginine amino acids, responsible for the more positive charge.

To further confirm the outcome of the different conjugation steps, we characterized the NPs by KBr-Fourier transform infrared spectroscopy (FTIR), transmission electron microscopy (TEM), fluorescence, and elemental analyses. PEGylation was further confirmed by KBr-FTIR spectra (Figure S1B, Supporting Information), in which we see the amide–indicative bands at 1565–1570 cm^{-1} (in-plane N–H bending and C–N stretching) and 1630–1640 cm^{-1} (amide C=O stretching). The conjugation of lin-TT1 and ANP peptides did not change the FTIR spectrum, thus further methods were used to confirm the successful conjugation of the peptides onto the NP's surface. The presence of lin-TT1 was detected by fluorescence microscopy (data not shown), since the peptide was conjugated to a carboxyfluorescein (FAM) moiety. Conjugation with ANP instead, was confirmed by elemental analysis, which revealed the presence of 41.06 μg of ANP in 1 mg of Putre-AcDEX-PEG-TT1-ANP NPs. Morphology of the NPs was examined by TEM. As shown by images in Figure S1C (Supporting Information), NPs have a spherical shape, with a diameter comprised between 100 and 200 nm, slightly smaller than what was observed with dynamic light scattering (DLS). This phenomenon is explained by the difference between TEM and DLS: while TEM is measuring diameter of dry NPs, DLS measures the hydrodynamic size of NPs.[28]

Since all in vitro studies were performed in cell medium and the NPs were later injected into rats for in vivo studies, we also investigated the colloidal stability of Putre-AcDEX NPs in cell medium containing serum and human plasma. The stability was also evaluated in an isotonic solution of sucrose, which was used for the resuspensions of NPs before being injected in rats. The PDI value was recorded just for studies in cell medium and isotonic sucrose, since plasma was presenting several peaks corresponding to different proteins, which are part of its composition.

As shown in **Figure 1**, Putre-AcDEX-PEG-TT1-ANP NPs have higher stability up to 2 h, both in terms of size (Figure 1A) and PDI (Figure 1B), compared to Putre-AcDEX NPs in Dulbecco's Modified Eagle's Medium (DMEM)/F-12 containing 10% of fetal bovine serum (FBS) (Figures 1A,B). This is explained by the anti-fouling properties of PEG, which has been extensively used to increase the stability of NPs.[29–31] However, the stealth properties of PEG were not remarkable here, since the PEG used has a short chain and it is known that the increase of the colloidal stability by PEG is affected by the length of the PEG used and its grafting density.[29,30] Size and PDI values of Putre-AcDEX NPs in isotonic sucrose (Figures 1C,D) did not vary up to 2 h, showing that the NPs' suspensions were stable under the conditions tested. Finally, stability tests of Putre-AcDEX NPs in plasma (Figure 1E) showed again that NPs conjugated with both lin-TT1 and ANP had better stability compared to bare NPs.

2.2. Biocompatibility Studies on Primary CMs and FBs

The biocompatibility of Putre-AcDEX NPs was assessed in vitro on both primary rat CMs and fibroblasts (FBs). Considering that previous studies with these NPs were performed on macrophages of murine and human origin, we decided to study the safety of the system also on murine primary CMs and human induced pluripotent stem cell (hiPSC)-derived CMs (hiPSC-CMs) to confirm that the results were comparable between species.

Cytocompatibility was studied by luminescence detection of the adenosine triphosphate (ATP) present in cell culture with a CellTiter-Glo luminescence assay, which quantifies the number of viable cells.[32] Primary CMs and FBs were incubated with the particles and cell viability was evaluated after 24 and 48 h. Since the stimulation of CMs proliferation by re-entry in the cell cycle obtained with the compounds CHIR99021 and SB203580 (abbreviated as CHIR and SB, respectively) takes time to manifest, we chose long time-points for determination of the cell viability. As shown in **Figure 2**, Putre-AcDEX NPs are biocompatible both toward primary CMs (Figures 2A,B) and FBs (Figure 2C,D) for 24 and 48 h.

Bare Putre-AcDEX NPs, which are highly positively charged, did not show toxicity toward cardiac cells, despite it is known that positively charged NPs usually show some degree of toxicity.[33] Toxicity of positively charged particles derives from their increased interaction with the negatively charged cell membranes. As a result, the plasma-membrane integrity is disrupted, high number of autophagosomes are produced and cellular organelles, in particular mitochondria and lysosomes are damaged.[33] Finally, loading of the NPs with CHIR and SB, resulted in improved safety for both nanocarriers, indicating a protective effect of the drugs on the cells.

Next, we assessed the cytocompatibility on primary murine CMs (Figures S2A,B, Supporting Information) and hiPSC-CMs (Figures S3A,B, Supporting Information). Also in this case, both

© 2023 The Authors. Advanced Functional Materials published by Wiley-VCH GmbH

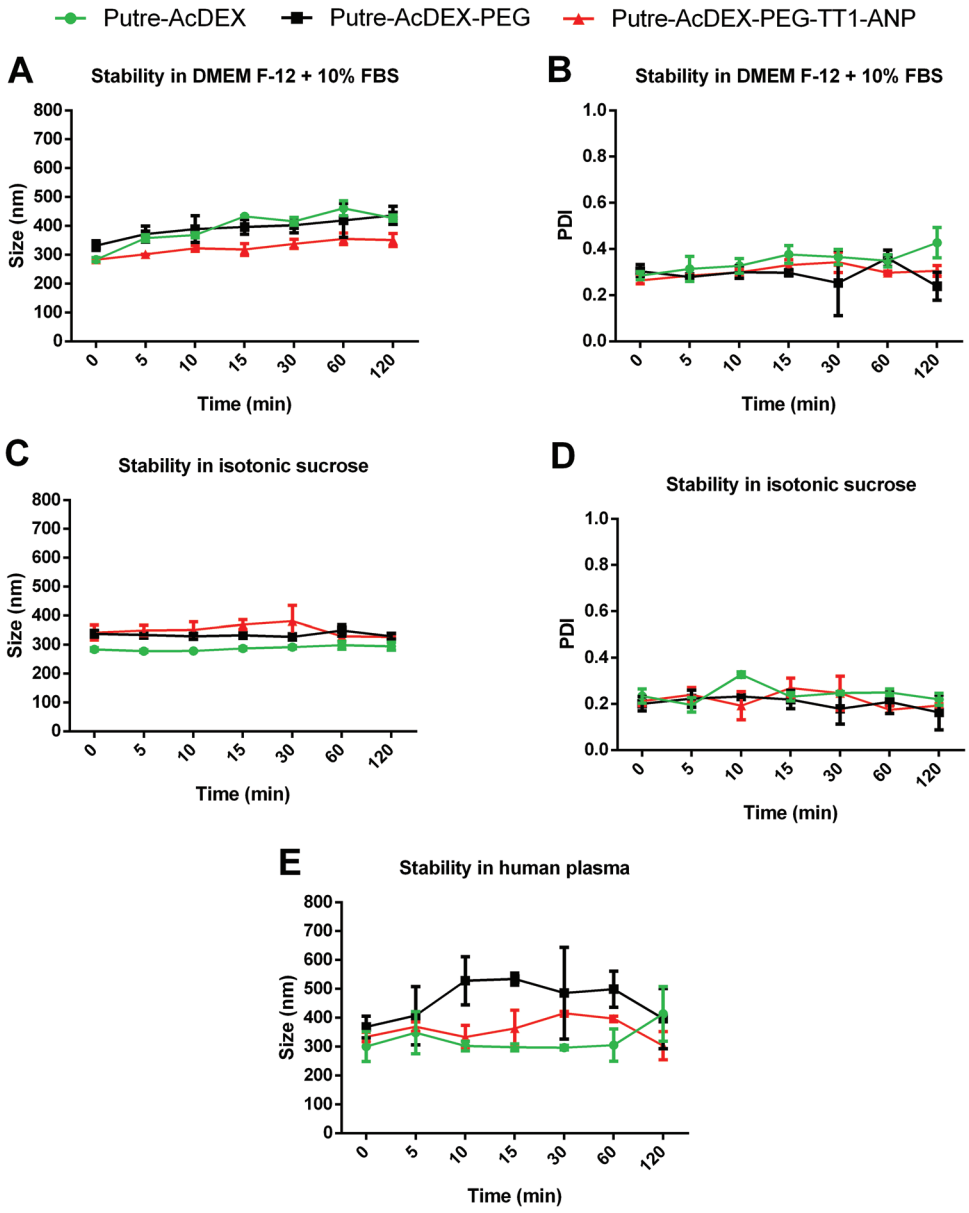

Figure 1. Evaluation of the colloidal stability of Putre-AcDEX NPs in different media. Stability studies were performed by recording size (A) and PDI (B) in DMEM F-12 + 10% FBS, isotonic sucrose (C and D) and in human plasma (E). Values are represented as the mean ± standard deviation (S.D.) ($n \geq 3$ biological replicates in which each time three technical replicates were used).

Putre-AcDEX and Putre-AcDEX-PEG-TT1-ANP NPs, showed to be safe toward CMs, with the exception of Putre-AcDEX NPs in murine CMs for 48 h (Figure S2B, Supporting Information). In that condition there was a dose-dependent toxicity of Putre-AcDEX NPs, probably attributable to the positive charge of the NPs and higher sensitivity of murine CMs.

2.3. Study of the Nanoparticle Interaction with Primary Cardiac Cells

Interaction of Putre-AcDEX NPs with cardiac cells was investigated in vitro both quantitatively and qualitatively. Cells were incubated for 2 h with fluorescently labelled NPs and the cell uptake was then quantified by flow cytometry. As shown in **Figure 3**A, NPs conjugated with both peptides have significantly higher uptake in CMs than PEGylated NPs. The higher uptake of Putre-AcDEX-PEG-TT1-ANP NPs can be due to their positive charge, which makes them interact more with negatively charged cell membranes, but it is due also to the presence of ANP on the NPs' surface. In order to understand whether the interaction was dictated by the binding of ANP to its receptors expressed on the CMs' surface, cells were pre-treated with free ANP for 30 min in order to saturate receptors, and then the NPs were added without removing the free ANP solution to avoid their turn-over. It is known that the binding of ANP to its receptor can be saturable

© 2023 The Authors. Advanced Functional Materials published by Wiley-VCH GmbH

16163028, 0, Downloaded from https://onlinelibrary.wiley.com/doi/10.1002/adfm.202303658 by University of Turku, Wiley Online Library on [31/05/2023]. See the Terms and Conditions (https://onlinelibrary.wiley.com/terms-and-conditions) on Wiley Online Library for rules of use; OA articles are governed by the applicable Creative Commons License

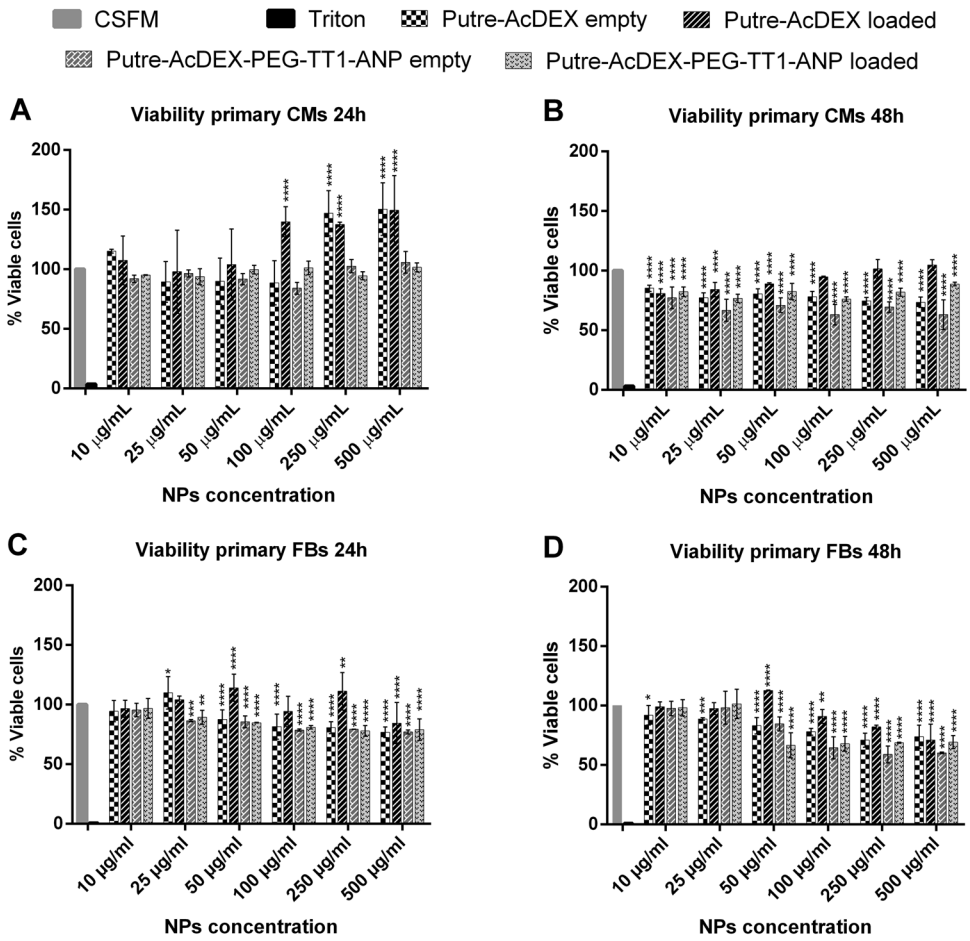

Figure 2. Biocompatibility of Putre-AcDEX NPs on primary rat CMs and FBs. Cytocompatibility studies were conducted to assess the safety of the produced nanoparticles on both primary rat CMs (A, B) and FBs (C, D) for 24 (A, C) and 48 h (B, D). Values are represented as mean ± S.D. ($n = 3$ biological replicates in which each time three technical replicates have been used). A one-way ANOVA followed by a Tukey–Kramer post hoc test was used for the statistical analysis. The significance levels of the differences were set at probabilities of $*p < 0.05$, $**p < 0.01$, $***p < 0.001$, and $****p < 0.0001$ for comparison with the medium, which was used as control in all tests.

and that the receptor is then recycled on the cell membrane of the cells.[34] As shown in Figures 3A,B, the pre-treatment with free ANP was able to significantly reduce the uptake of Putre-AcDEX-PEG-TT1-ANP NPs, demonstrating that part of the interaction with CMs is due to presence of ANP on the NP's surface. For FBs (Figures 3C,D), the conjugation with the peptides also enhanced the interaction of the NPs with the cells. However, pre-treatment with ANP did not reduce the uptake of the NPs, suggesting that NPs were taken up by the FBs non-specifically. Moreover, NPs interacted more with primary CMs compared to FBs, since after conjugation with the peptides the percentage of CMs interacting with Putre-AcDEX-PEG-TT1-ANP NPs was approximately double that of the FBs.

We then qualitatively evaluated the uptake of Putre-AcDEX NPs by confocal imaging. We studied the uptake in both murine and rat primary CMs and in hiPSC-CMs. As shown in Figures S3–S5 (Supporting Information), Putre-AcDEX-PEG-TT1-ANP NPs showed a greater interaction with the cells compared to PEGylated NPs, confirming the quantitative results discussed above. Also here, we investigated the effects of free ANP pre-treatment on NP uptake, and the images supported flow cytometry results, displaying less NPs, which are shown in green in the AlexaFluor 488® (a trademark from Thermofisher Scientific) channel.

Overall, the peptide-modified NPs present an ANP-driven interaction with cardiac cells, which was exploited synergistically with macrophages hitchhiking, in the in vivo studies described below.

2.4. Cardiomyocyte Proliferation Studies

The aim of the loaded compounds CHIR and SB was to stimulate CM proliferation synergistically, as previously reported.[12] We then assessed the ability of loaded Putre-AcDEX NPs to induce proliferation by incubating primary CMs for 24 h with different concentrations of empty and loaded NPs, corresponding to concentrations of CHIR 1, 3, 5, and 10×10^{-6} M (concentrations of SB are approximately double that of CHIR), calculated from the loading degree (LD) values of the drug. The LD values for drugs encapsulated in Putre-AcDEX-PEG-TT1-ANP NPs were ≈1 and 1.7% for CHIR and SB respectively, as calculated in our previous work.[21] Compounds alone were also used as

© 2023 The Authors. Advanced Functional Materials published by Wiley-VCH GmbH

16163028, 0, Downloaded from https://onlinelibrary.wiley.com/doi/10.1002/adfm.202303658 by University of Turku, Wiley Online Library on [31/05/2023]. See the Terms and Conditions (https://onlinelibrary.wiley.com/terms-and-conditions) on Wiley Online Library for rules of use; OA articles are governed by the applicable Creative Commons License

16163028, 0, Downloaded from https://onlinelibrary.wiley.com/doi/10.1002/adfm.202303658 by University of Turku, Wiley Online Library on [31/05/2023]. See the Terms and Conditions (https://onlinelibrary.wiley.com/terms-and-conditions) on Wiley Online Library for rules of use; OA articles are governed by the applicable Creative Commons License

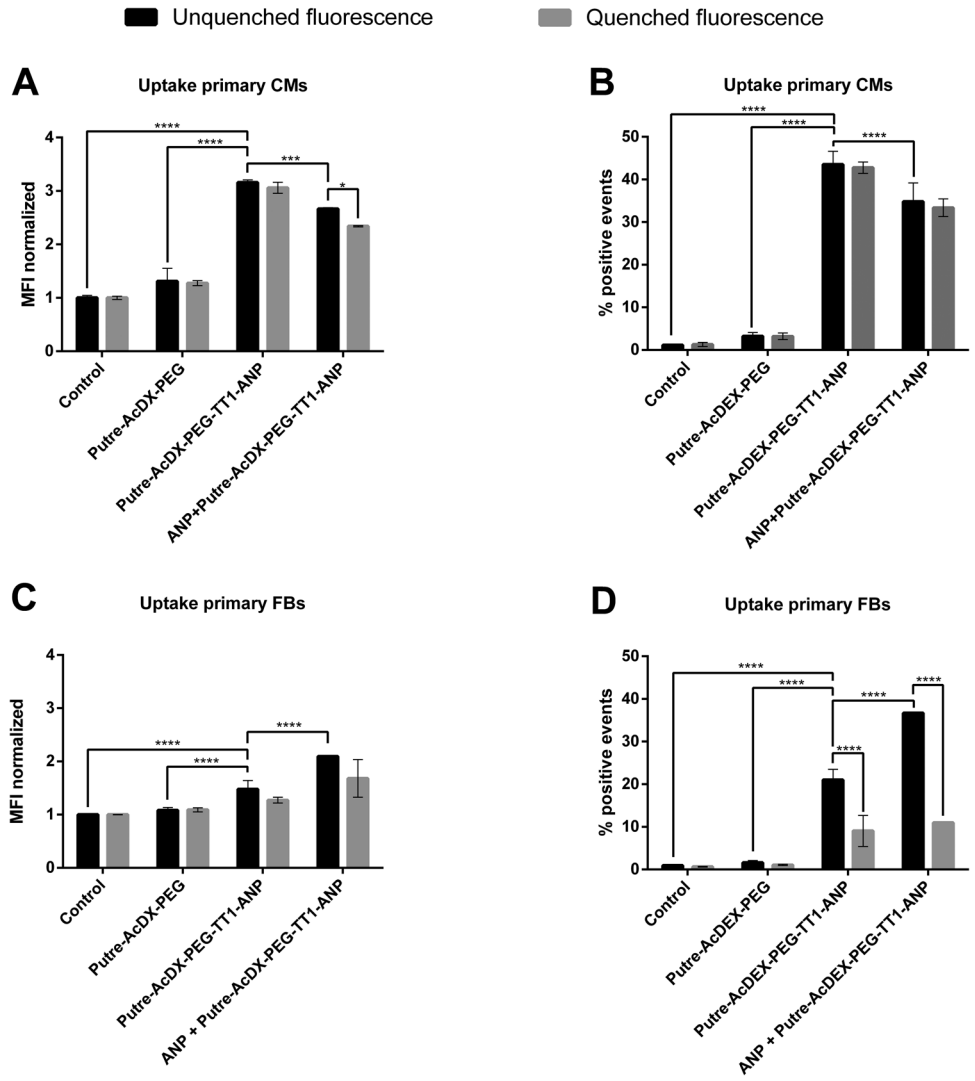

Figure 3. Quantitative cell uptake on primary rat cardiac cells. Interactions between Putre-AcDEX-based NPs and cells were studied on primary rat CMs (A, B) and FBs (C, D). Results are represented as median fluorescence intensity (MFI) values or % of positive events ± S.D. ($n = 3$ biological replicates in which each time three technical replicates have been used). A one-way ANOVA followed by a Tukey–Kramer post hoc test was used for the statistical analysis. The significance levels of the differences in uptake studies were set at probability of $^{****}p < 0.0001$ for comparison between Control, Putre-AcDEX-PEG and Putre-AcDEX-PEG NPs, and Putre-AcDEX-PEG-TT1-ANP NPs, and $^{***}p < 0.001$ for comparison between internalized unquenched fluorescence with or without treatment with ANP.

controls and the biological effects were evaluated by quantifying the percentage of BrdU positive cells, and the staining intensity of phospho-mitogen-activated protein kinase-activated protein kinase 2 (MAPKAPK2, downstream effector of p38 inhibition by SB)[35] and β-catenin (downstream effector of CHIR).[36] For murine primary CMs and hiPSC-CMs, we chose the concentration of CHIR 5×10^{-6} M, since it was the one showing better results for compounds loaded in Putre-AcDEX-PEG-TT1-ANP NPs for rat CMs and was corresponding to still safe concentration of NPs. After 24 h of incubation, cells were fixed and immunostained for nuclei (4′,6-diamidino-2-phenylindole, DAPI), BrdU, phospho-MAPKAPK2 or β-catenin, and in addition for a CMs marker (cardiac troponin T), which allowed to select the cells of interest from the primary culture. The quantification of percentage of BrdU positive cells, phospho-MAPKAPK2 and β-catenin intensities was done by high content imaging by choosing regions of interest corresponding to the nucleus and the cytoplasm (DAPI staining was used to define the nuclear area and a 5-pixel ring immediately outside the nucleus was considered to represent cytoplasm).

As shown in **Figure 4**A,B, after treatment with Putre-AcDEX-PEG-TT1-ANP NPs corresponding to concentration of CHIR of 5×10^{-6} M, the percentage of BrdU positive cells was 4 times higher than after treatment with empty NPs (control) before and after surface conjugations, as well as loaded Putre-AcDEX NPs. The NPs at this concentration thus hold potential of being able to stimulate proliferation of CMs.

Next, we investigated the modulation of downstream effectors of Wnt activation by CHIR and p38 inhibition by SB. Inhibition of p38 by SB has been reported to modulate

 © 2023 The Authors. Advanced Functional Materials published by Wiley-VCH GmbH

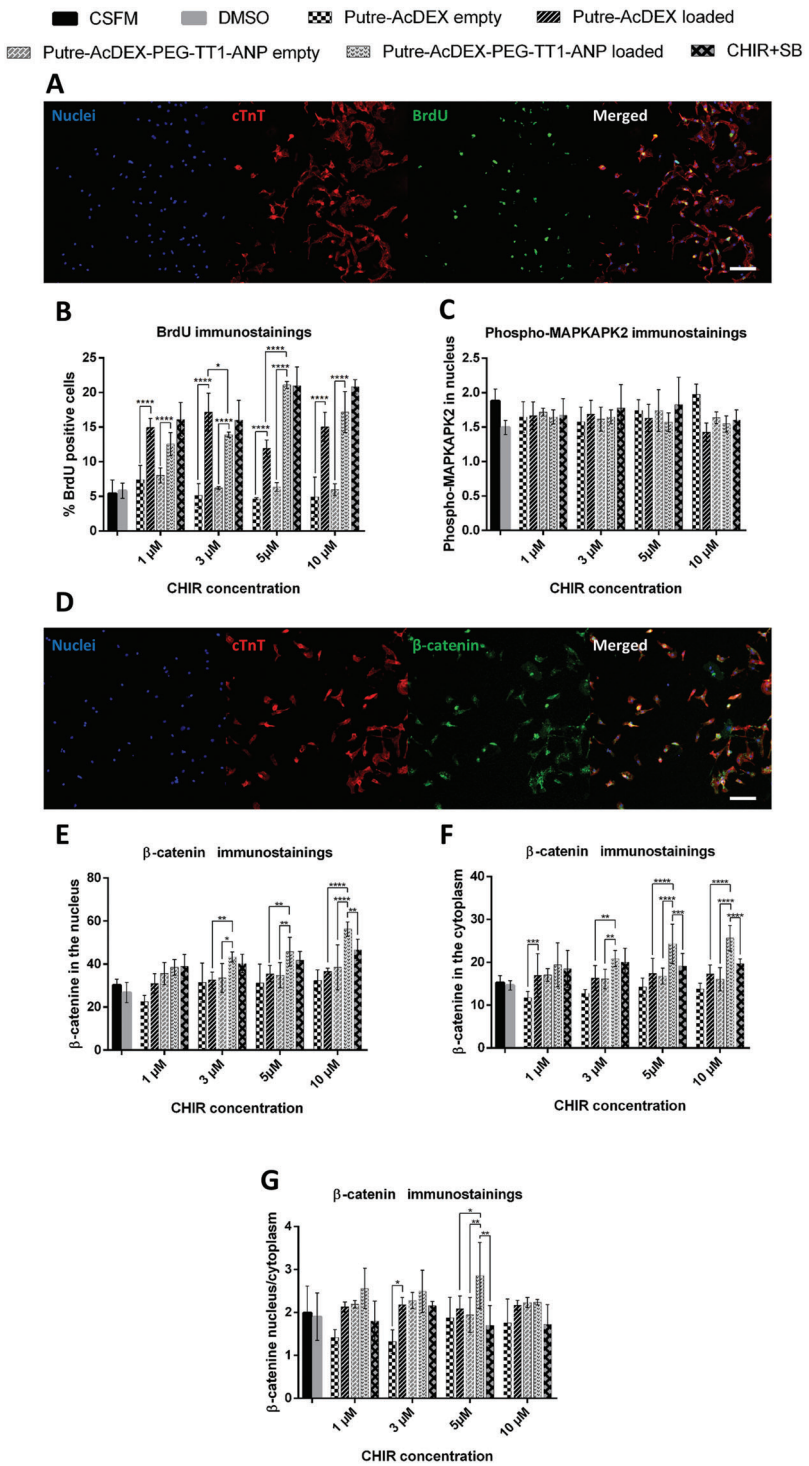

Figure 4. High-content cell imaging and quantification of BrdU, phospho-MAPKAPK2, and β-catenin staining intensity and sub-cellular localization in primary rat CMs. Representative images of primary rat CMs (A) treated with loaded Putre-AcDEX-PEG-TT1-ANP NPs at the concentrations of 5 μM of CHIR99021 and 10 μM of SB203580, and stained for nuclei (DAPI, blue), cardiac troponin T (cTnt, red) and BrdU (green), with a 10× magnification objective. Scale bars are 200 μm. B) Quantification of percentage of BrdU positive cells. C) Quantification of phospho-MAPKAPK2 staining intensity in the nucleus. Representative images of primary rat CMs (D) treated with loaded Putre-AcDEX-PEG-TT1-ANP NPs at the concentrations of 5 μM of CHIR99021 and 10 μM of SB203580, and stained for nuclei (DAPI, blue), cardiac troponin T (cTnt, red) and β-catenin (green), with a 10× magnification objective. Scale bars are 200 μm. Quantification of β-catenin staining intensity in the nucleus (E), in the cytoplasm (F), and the ratio of β-catenin in nucleus/cytoplasm (G). Values are represented as mean ± S.D. ($n = 3$ biological replicates in which each time three technical replicates have been used). A one-way ANOVA followed by a Tukey–Kramer post hoc test was used for the statistical analysis. The significance levels of the differences were set at probabilities of $^{*}p < 0.05$, $^{**}p < 0.01$, $^{***}p < 0.001$, and $^{****}p < 0.0001$ for comparison between loaded Putre-AcDEX and Putre-AcDEX-PEG-TT1-ANP NPs and among empty and loaded NPs.

© 2023 The Authors. Advanced Functional Materials published by Wiley-VCH GmbH

16163028, 0, Downloaded from https://onlinelibrary.wiley.com/doi/10.1002/adfm.202303658 by University of Turku, Wiley Online Library on [31/05/2023]. See the Terms and Conditions (https://onlinelibrary.wiley.com/terms-and-conditions) on Wiley Online Library for rules of use; OA articles are governed by the applicable Creative Commons License

expression of genes required for mitosis in CMs, including cyclin A and cyclin B,[13] as well as to play an important role during late phases of cytokinesis.[37] Activation of p38 leads to a series of phosphorylation events activating different MAPKs, which then translocate into the nucleus and induce transcription of specific genes.[13] We therefore assessed the inhibition of p38 by studying the decrease of phospho-MAPKAPK2 in the nucleus. As shown by Figure 4C, a slight decrease of Phospho-MAPKAPK2 fluorescence intensity in the nucleus of cells treated with loaded Putre-AcDEX-PEG-TT1-ANP NPs at the concentration CHIR of 5×10^{-6} M was observed, but this change was not statistically significant.

Activation of Wnt/β-catenin signaling pathway by CHIR, which has an important role in cardiac development and proliferation,[36,38] was analyzed as an increase of β-catenin staining in cytoplasm and nucleus. CHIR acts as an inhibitor of the glycogen synthase kinase 3 (GSK3), preventing β-catenin phosphorylation and its further degradation, subsequently allowing its translocation in the nucleus for regulating expression of target genes.[36] As shown in Figure 4D,E, treatment with loaded Putre-AcDEX-PEG-TT1-ANP NPs at 3, 5, and 10×10^{-6} M concentrations of CHIR, induced significant increase in β-catenin staining intensity in the nucleus compared to empty Putre-AcDEX-PEG-TT1-ANP NPs and loaded Putre-AcDEX NPs. An increase of β-catenin was reported also in the cytoplasm (Figure 4D–F), when cells were treated with loaded Putre-AcDEX-PEG-TT1-ANP NPs compared to empty Putre-AcDEX-PEG-TT1-ANP NPs (for CHIR concentrations of 3, 5, and 10×10^{-6} M, respectively) and loaded Putre-AcDEX NPs (for CHIR concentrations of 3, 5, and 10×10^{-6} M, respectively). The nucleus to cytoplasm ratio of β-catenin (Figure 4D–G) differed statistically significantly for Putre-AcDEX-PEG-TT1-ANP NPs compared to empty putre-AcDEX-PEG-TT1-ANP NPs ($p < 0.05$) and loaded Putre-AcDEX NPs ($p < 0.01$) for the concentration CHIR 5×10^{-6} M.

Similar results were obtained with murine primary CMs and hiPSC-CMs, treated with NPs and compounds at concentrations corresponding to CHIR 5×10^{-6} M (Figures S6 and S7, respectively, Supporting Information). Primary murine CMs, showed similar percentages of positive BrdU cells (Figure S6A,B, Supporting Information) to rat primary CMs for loaded Putre-AcDEX-EPG-TT1-ANP NPs. However, there were no statistically significant differences between percentages of BrdU positive CMs when cells were treated with loaded Putre-AcDEX NPs and loaded Putre-AcDEX-EPG-TT1-ANP NPs. For phospho-MAPKAPK2 immunostainings, murine CMs exhibited a decrease of staining intensity in the nucleus for loaded NPs compared to empty ones, but values were not significantly different (Figure S6C, Supporting Information). Murine CMs also showed an increase in β-catenin staining intensities in both nucleus (Figure S6D,E, Supporting Information) and cytoplasm (Figure S6D,F, Supporting Information) in a comparable way to rat CMs. However, differences in the nucleus to cytoplasm ratio of β-catenin (Figure S6D,G, Supporting Information) between the different groups were not statistically significant.

For the human counterpart, hiPSC-CMs, similar trends were observed. For BrdU immunostainings, percentages of BrdU positive cells were lower compared to rat and murine CMs (Figure S7A,B, Supporting Information). Also, there were no statistically significant differences between cells treated with Putre-AcDEX NPs and Putre-AcDEX-PEG-TT1-ANP NPs. However, there were statistically significant differences when the drug-loaded Putre-AcDEX and Putre-AcDEX-PEG-TT1-ANP NPs were compared with cells treated with DMSO, suggesting that lower BrdU incorporation values could be a consequence of cellular stress caused by the DMSO.[39] For phospho-MAPKAPK2 immunostainings (Figure S7C, Supporting Information), hiPSC-CMs showed a decrease in staining intensity in the nucleus for loaded NPs compared to empty ones, as well as when compared to controls. Comparable results were observed also for β-catenin immunostainings, where the staining intensity was higher in both nucleus (Figure S7D,E, Supporting Information) and cytoplasm (Figure S7D,F, Supporting Information) for cells treated with loaded Putre-AcDEX-PEG-TT1-ANP NPs compared to their empty counterpart and bare loaded Putre-AcDEX NPs. Also, for hiPSC-CMs, there was no statistically significant nucleus-to-cytoplasm ratio of β-catenin (Figure S7D,G, Supporting Information) for the NPs, except for the comparison between empty and loaded Putre-AcDEX NPs and the one between DMSO and loaded Putre-AcDEX NPs.

Overall, these results show that the NPs are suitable for modulation of p38 and β-catenin signaling pathways and intracellular delivery of hydrophobic CHIR and SB for the stimulation of CMs proliferation in cells of rat, murine and human origin.

2.5. Evaluation of the Phenotype Change in Murine M1– and M2–Like Macrophages Treated with the NPs

Evaluation of the phenotype of M1– and M2–like macrophages after treatment with Putre-AcDEX NPs was performed by studying the expression of markers on the cells after incubation with the NPs at different time-points. Given the hitchhiking effect of the system on macrophages, it is important to study how the interaction of these cells with the NPs is influencing their phenotype. The compounds encapsulated in the NPs, CHIR and SB, have shown anti-inflammatory properties.[40,41] GSK3 inhibition by CHIR is known to result in reduced serum level of tumor necrosis factor alpha (TNF-α) and increased anti-inflammatory interleukin 10 (IL-10) protein level.[40] Also, inhibition of the GSK decreases the expression of markers genes, such as CD11c, CD68, and F4/80 and the pro-inflammatory cytokine/chemokine genes like Tnfa, IL-1b, Mcp-1, and -3.[40] Inhibition of p38 MAPK by SB results in decrease of the lipopolysaccharide (LPS)-induced secretion of TNF-α and IL-6.[41] The ANP peptide has also shown immunomodulatory effects.[42] In particular, it was demonstrated that ANP reduces the secretion of inflammatory mediators in macrophages by inhibiting the LPS-induced expression of inducible nitric oxide synthase (iNOS), and the secretion of TNF-α and IL1-β in macrophages.[42]

As shown in **Figures 5**A,B, treatment with drug loaded Putre-AcDEX-PEG-TT1-ANP (nanoformulation abbreviated as Final L in Figure 5) reduced the expression of CD86 in M1-like macrophages when NPs were in contact with the cells for 1 h. The effect was reduced when cells were incubated with the NPs for 2 h, suggesting a transient modulation of the marker expression. We hypothesize that the fast polarization effect is triggered by combinatory effects of the interaction between ANP and its receptor on the surface of macrophages,[43] and lin-TT1

© 2023 The Authors. Advanced Functional Materials published by Wiley-VCH GmbH

16163028, 0, Downloaded from https://onlinelibrary.wiley.com/doi/10.1002/adfm.202303658 by University of Turku, Wiley Online Library on [31/05/2023]. See the Terms and Conditions (https://onlinelibrary.wiley.com/terms-and-conditions) on Wiley Online Library for rules of use; OA articles are governed by the applicable Creative Commons License

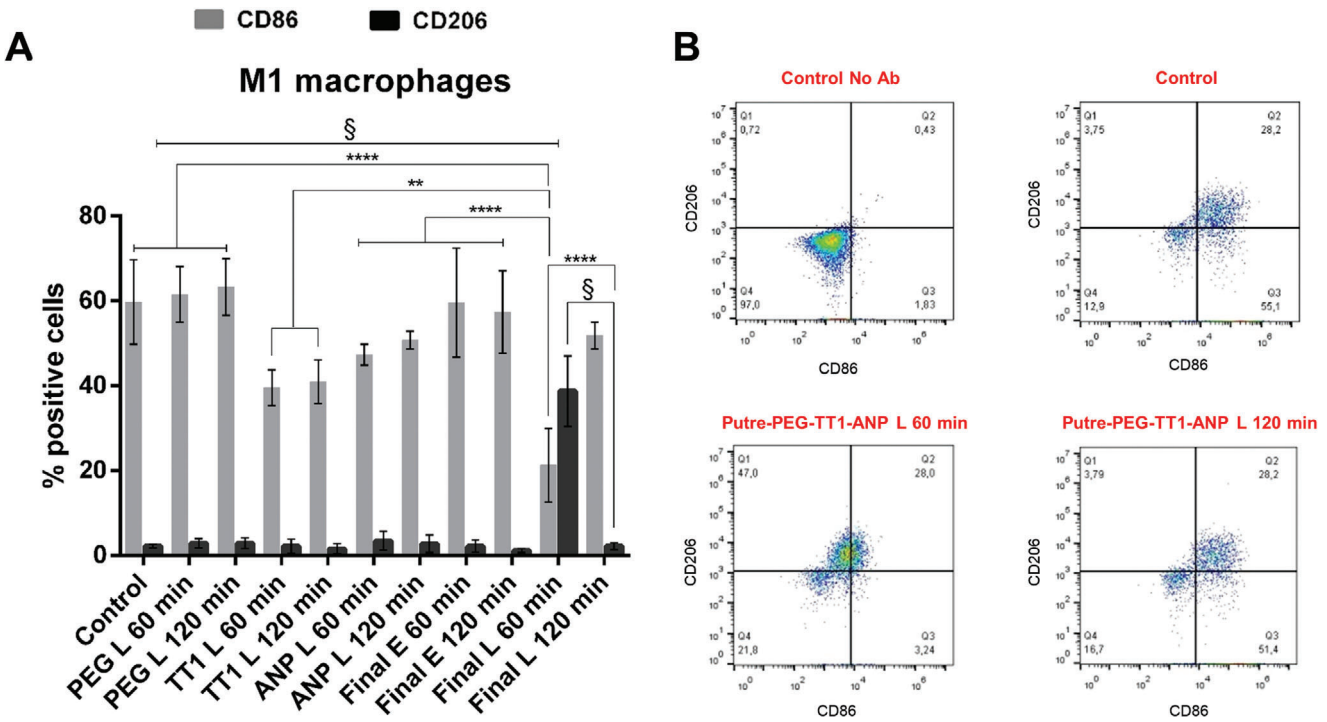

Figure 5. In vitro evaluation of the phenotype changes in M1-like macrophages. M1-like murine macrophages were screened for their marker's expression after treatment with different types of NPs for different time-points. A) The percentages of CD86 and CD206 expression were analyzed by flow cytometry (B). Results are represented as percentages of positive cells ± S.D. ($n = 3$ biological replicates in which each time three technical replicates have been used). A one-way ANOVA followed by a Tukey–Kramer post hoc test was used for the statistical analysis. The significance levels of the differences for CD86 were set at the probability of $^{****}p < 0.0001$ for comparison between all the conditions and drug loaded Putre-AcDEX-PEG-ANP (ANP L), except for empty and drug loaded Putre-AcDEX-PEG-TT1 NPs, which had a difference with a probability set of $^{***}p < 0.001$. The significance levels of the differences for CD206 were set at the probability of $^{§}p < 0.0001$ for comparison between all the conditions and drug loaded Putre-AcDEX-PEG-TT1-ANP (Final L) incubated with the cells for 1 h.

peptide with Neuropilin-1 (NRP-1).[44] Both stimulation of NRPs and NRP-1 are reported to induce an anti-inflammatory phenotype on macrophages. PEGylated particles did not show ability to significantly decrease the expression of CD86 in M1–like macrophages, while particles with only one peptide (Putre-AcDEX-PEG-TT1 and Putre-AcDEX-PEG-ANP) showed less ability to reduce their inflammatory phenotype. In particular, particles conjugated with ANP only showed a better ability to reduce the expression of CD86 compared to the ones having only lin-TT1 on their surface, indicating that both drugs encapsulated and ANP have a role in reducing the inflammatory phenotype of M1–like macrophages. Treatment with empty Putre-AcDEX-PEG-TT1-ANP showed the contribution of ANP in reducing the CD86 expression in M1-like macrophages. The encapsulated compounds and the ANP peptide had then a synergistic anti-inflammatory effect toward M1–like macrophages. Also, as shown in Figures 5A,B, treatment with the drug loaded Putre-AcDEX-PEG-TT1-ANP NPs for 1 h increased the expression of CD206 in M1-like macrophages, reinforcing the evidence of the anti-inflammatory effect discussed above. Figure S8 (Supporting Information) instead shows the markers' expression in M2-macrophages with no statistically significant changes between the different conditions tested. This indicates that the final nanosystem composed by drug-loaded NPs conjugated with both the peptides has anti-inflammatory properties.

Overall, considering these results and the previous in vitro studies[21] have demonstrated that Putre-AcDEX-PEG-TT1-ANP NPs have higher association versus uptake for M2-like macrophages, we hypothesize that the anti-inflammatory phenotype change induced by the system in M1-like macrophages can ultimately enhance the accumulation of the NPs in the infarcted site.

2.6. Ex Vivo Biodistribution Studies and Immunoprofiling

The ability of Putre-AcDEX-PEG-TT1-ANP NPs to reach the infarcted myocardium and deliver payloads for potential regeneration of the damaged tissue, was assessed by in vivo biodistribution studies, in which fluorescently labelled NPs were injected intravenously (IV) into rats from the tail vein. Animals were divided into four groups, namely isotonic sucrose, Putre-AcDEX-PEG, Putre-AcDEX-PEG-ANP, and Putre-AcDEX-PEG-TT1-ANP NPs (n = 5). NPs or vehicle alone were injected after 3 or 7 days post-MI, which was induced by ligation of the left anterior descending coronary artery (LAD). These two time points were chosen considering that they represent the peak of M1– and M2–like macrophages into the infarcted area, respectively.[26] Animals were sacrificed 1 h after injecting the NPs and organs were

© 2023 The Authors. Advanced Functional Materials published by Wiley-VCH GmbH

16163028, 0, Downloaded from https://onlinelibrary.wiley.com/doi/10.1002/adfm.202303658 by University of Turku, Wiley Online Library on [31/05/2023]. See the Terms and Conditions (https://onlinelibrary.wiley.com/terms-and-conditions) on Wiley Online Library for rules of use; OA articles are governed by the applicable Creative Commons License

collected and sectioned to study the NPs accumulation by confocal microscopy.

Images of sectioned infarcted hearts taken from animals injected with the NPs at 3 (**Figure 6**A) and day 7 (Figure 6B) after MI showed that the NPs conjugated with both peptides, Putre-AcDEX-PEG-TT1-ANP NPs, accumulated in the heart preferentially at day 7 post-MI.

From the images, it can also be observed that Putre-AcDEX-PEG-TT1-ANP accumulated more in the heart compared to Putre-AcDEX-PEG-ANP NPs, showing that conjugation with lin-TT1 peptide helped to increase the heart target ability of ANP. Co-localization of the NPs together with the staining of the inflammatory cells markers, shown in yellow color in the images due to overlapping of the green channels of the NPs and the red channel of the CD163, indicate that the NPs accumulate in the infarcted hearts due to the interaction with inflammatory cells. NPs did not show a high accumulation in the hearts of sham-operated (SHAM) animals (Figure S9, Supporting Information). In addition to the heart, NPs also accumulated in the liver (Figure S10, Supporting Information) and the spleen (Figure S11, Supporting Information), while lung accumulation was minimal (Figure S12, Supporting Information), indicating that the formulation did not show instability and aggregation upon intravenous administration. Accumulation of NPs in the liver and spleen instead is typical and due to complexation of NPs by cells of the reticuloendothelial system (RES).[45] Notably, all NPs (PEGylated, conjugated only with ANP and with both peptides) accumulated more in the spleen compared to liver, probably as result of their size and spleen's loose capillaries or in case of TT1 modified NPs because of their macrophage targeting ability.[46,47]

Since Putre-AcDEX-PEG-TT1-ANP NPs were interacting with inflammatory cells due to the presence of lin-TT1 peptide, we evaluated the immunoprofile of spleens and white cells derived from the animals' blood to exclude any possible toxic effects of the NPs. Inflammatory cells were extracted from the tissues and the red blood cells were eliminated osmotically, followed by staining for different macrophage and T-cells markers. Percentages of cells expressing the different markers were then quantified by flow cytometry.

As shown in **Figure 7**, there were no statistically significant changes in the markers expression of macrophages at day 3 (Figure 7A) and 7 (Figure 7B), with exception of a reduction at day 7 post-MI (Figure 7B) of M1–like macrophages in spleens when animals were injected with NPs conjugated with only ANP and both TT1 and ANP peptides, and an increase of M2–like macrophages in animals injected with Putre-AcDEX-PEG-TT1-ANP NPs. These results are explained by the anti-inflammatory properties of both ANP[42] and the compounds encapsulated in the NPs,[40,41] as demonstrated by the in vitro studies above. For the T-cells, no statistically significant changes were found in the spleen and blood, except for a reduction in circulating $CD8^+$ T-cells at day 3 (Figure 7C) and a reduction in splenic $CD4^+$ T-cells at day 7 (Figure 7D) in animals injected with Putre-AcDEX-PEG-ANP NPs.

The role of T-cells in MI has not yet been completely elucidated, but some evidence has shown that $CD8^+$ T-cells are recruited into the myocardium following MI and they release granzyme B after activation. In this way, $CD8^+$ T-cells fostered adverse ventricular remodeling with their pro-apoptotic functions.[48] Studies with a $Cd8^{atm1mak}$ mice, a genetically modified mouse model characterized by CD8+ T-cell deficiency, have been shown that $CD8^+$ T-cells play a dual and contradictory role. In these studies, animals lacking functional $CD8^+$ T-cells had increased cardiac rupture despite having better overall survival after MI.[49] Other studies describe the presence of a subset of protective $CD8^+$ T-cells expressing the type 2 angiotensin II (ATII) receptor.[49] $CD4^+$ T-cells instead are activated in MI as a response to autoantigens and take part in wound healing, resolution of the inflammation and scar formation, limiting adverse remodeling.[50,51]

Our findings suggest that the Putre-AcDEX-PEG-ANP NPs have ability to reduce both $CD4^+$ and $CD8^+$ T-cells. This effect can be attributed to the ANP effect on T-cells.[52] It has been demonstrated that ANP reduces the number of lymphocytes $CD4^+$ $CD8^+$ while increasing the $CD4^-$ $CD8^-$ cells.[52] In SHAM-operated animals, trends were similar, showing an increase of M2–like macrophages at day 3 (Figure S13A, Supporting Information) and a reduction in M1–like macrophages at day 7 (Figure S13B, Supporting Information) when animals were treated with ANP conjugated NPs. For the T-cells instead, no statistically significant differences were observed, except for an increase in splenic $CD8^+$ T-cells at day 7 in animals injected with Putre-AcDEX-PEG-ANP NPs. However, differences were not statistically significant and there was not a consistent trend.

Overall, the NPs did not show any acute toxicity on inflammatory cells and demonstrated to be safe to the animals after injection.

2.7. In Vivo Positron Emission Tomography (PET) Studies and Evaluation of the Cardiac Function

As showed above, the nanosystem developed here reduced the pro-inflammatory phenotype of murine macrophages and was able to stimulate the proliferation of primary CMs in vitro. Next, we performed an in vivo pilot study to investigate the potential therapeutic effects of the designed nanosystem both in terms of reduction of the inflammation after MI, and in terms of improving the cardiac function.

In a clinical setting, the reduction of inflammation after MI has been shown to have beneficial effects on the cardiac outcome post-MI.[53–56] In order to evaluate the potential in vivo anti-inflammatory effects of our nanoformulation, we evaluated the accumulation of aluminum fluoride-18-labeled 1,4,7-triazacyclononane-1,4,7-triacetic acid conjugated folate (^{18}F-FOL) by PET imaging. This tracer was chosen because of its ability to target and image activated macrophages, which accumulate in inflammatory sites, such as atherosclerotic plaques and infarcted hearts.[57,58] Both SHAM and LAD ligated animals were divided in two groups, receiving either the Putre-AcDEX-PEG-TT1-ANP NPs or the vehicle, isotonic sucrose. Considering the enhanced accumulation of the NPs conjugated with both peptides at day 7 post-MI, we decided to inject NPs at day 6, 7, and 8 post-MI to follow the peak accumulation of M2-like macrophages and hypothetically achieve the highest accumulation of NPs in the infarcted hearts. ^{18}F-FOL tracer was injected 7 and 15 days after the onset of MI to evaluate the recruitment of macrophages in the infarcted heart.

© 2023 The Authors. Advanced Functional Materials published by Wiley-VCH GmbH

16163028, 0, Downloaded from https://onlinelibrary.wiley.com/doi/10.1002/adfm.202303658 by University of Turku, Wiley Online Library on [31/05/2023]. See the Terms and Conditions (https://onlinelibrary.wiley.com/terms-and-conditions) on Wiley Online Library for rules of use; OA articles are governed by the applicable Creative Commons License

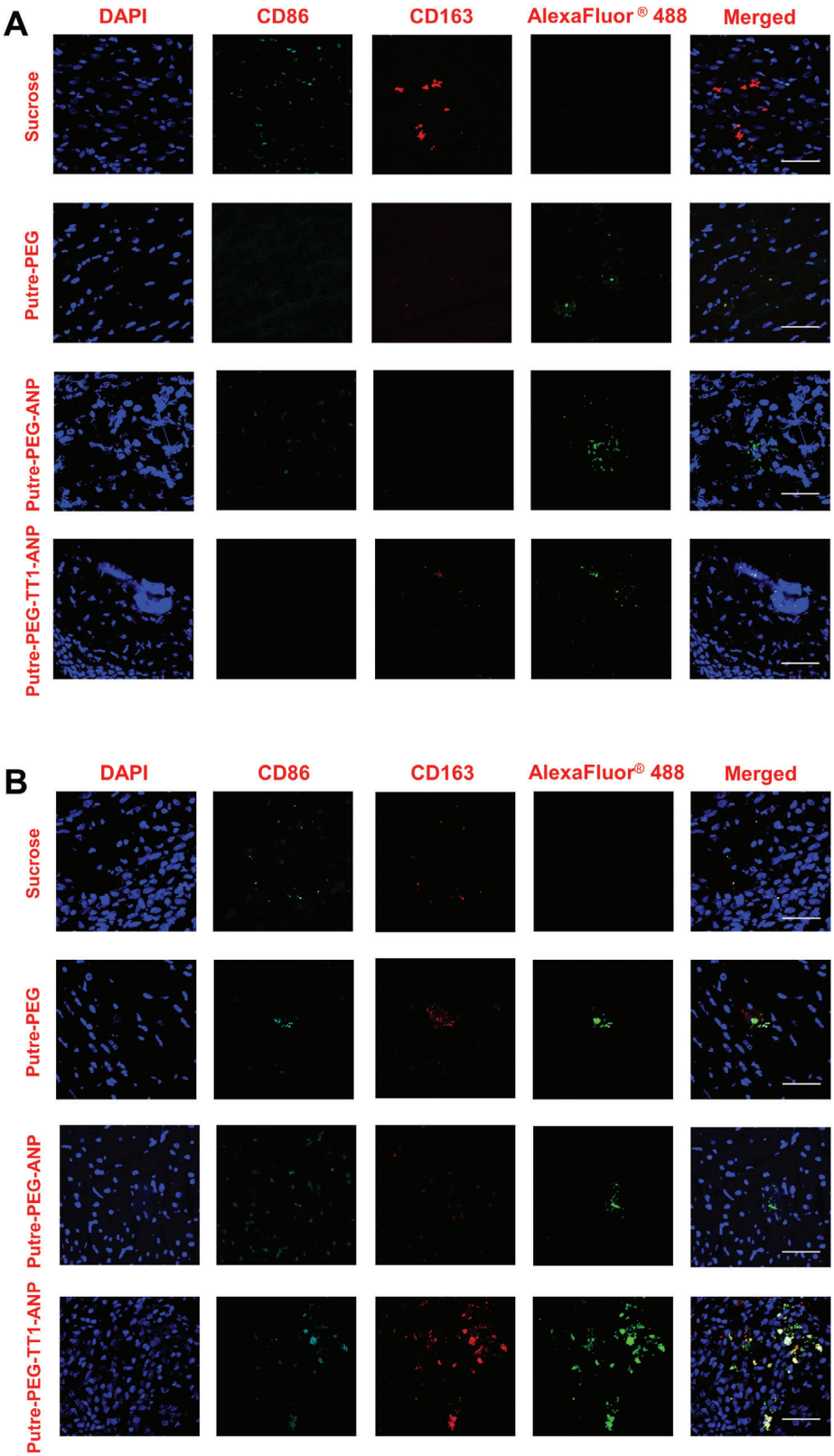

Figure 6. Ex vivo biodistribution of Putre-AcDEX-PEG-TT1-ANP NPs in infarcted hearts. Heart sections derive from animals injected with Putre-AcDEX NPs at day 3 (A) and day 7 (B) post-MI were stained and imaged by confocal microscopy. Scale bars are 200 µm.

© 2023 The Authors. Advanced Functional Materials published by Wiley-VCH GmbH

16163028, 0, Downloaded from https://onlinelibrary.wiley.com/doi/10.1002/adfm.202303658 by University of Turku, Wiley Online Library on [31/05/2023]. See the Terms and Conditions (https://onlinelibrary.wiley.com/terms-and-conditions) on Wiley Online Library for rules of use; OA articles are governed by the applicable Creative Commons License

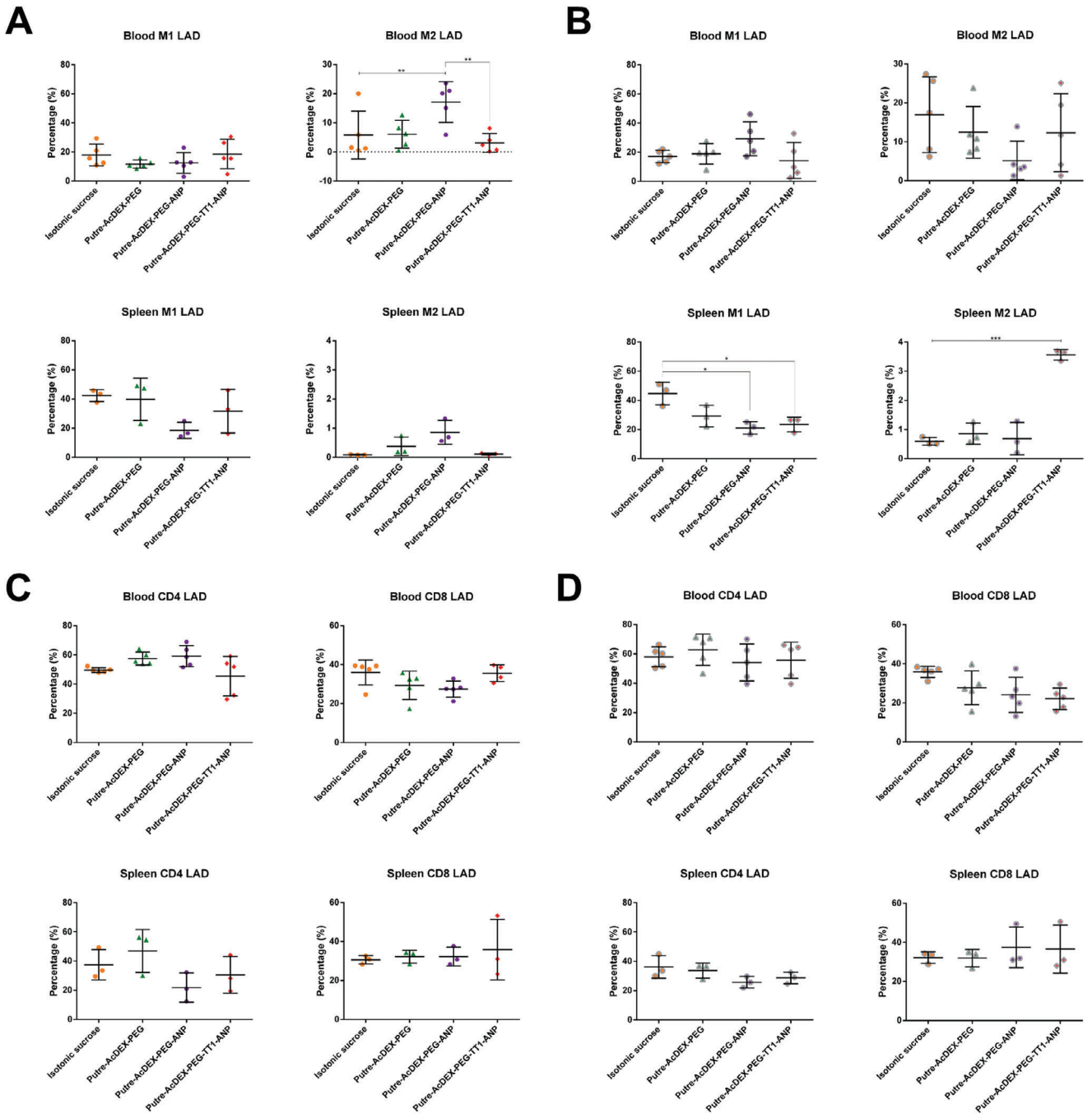

Figure 7. Immunoprofiling of spleen and blood from infarcted animals. A,B) The inflammatory cells derived from spleen and blood were stained for different macrophage, and (C,D) T-cells markers 3 days (A,C) and 7 days (B,D) post-MI. Results are represented as percentages of positive cells ± S.D. ($n = 3$ biological replicates in which each time three technical replicates have been used). A one-way ANOVA followed by a Tukey–Kramer post hoc test was used for the statistical analysis. The significance levels were set at probabilities of $^{*}p < 0.05$, $^{**}p < 0.01$, $^{***}p < 0.001$, and $^{****}p < 0.0001$ for comparison between the different conditions.

Figure 8A shows no statistically significant differences in tracer accumulation in the infarcted hearts between animals injected with vehicle or the NPs, and between the two different time points. However, despite not statistically significant, with the conditions tested we observed a reduction of tracer accumulation between 7 and day 15, when animals were treated with Putre-AcDEX-PEG-TT1-ANP NPs, indicating a potential in vivo anti-inflammatory effect of the NPs (Figures 8A; Figure S14A, Supporting Information).

Moreover, evaluation of the remodeling was studied by collecting echocardiography readings after 90 days from the onset of MI, and by evaluating the infarct size by hematoxylin and eosin

© 2023 The Authors. Advanced Functional Materials published by Wiley-VCH GmbH

16163028, 0, Downloaded from https://onlinelibrary.wiley.com/doi/10.1002/adfm.202303658 by University of Turku, Wiley Online Library on [31/05/2023]. See the Terms and Conditions (https://onlinelibrary.wiley.com/terms-and-conditions) on Wiley Online Library for rules of use; OA articles are governed by the applicable Creative Commons License

16163028, 0, Downloaded from https://onlinelibrary.wiley.com/doi/10.1002/adfm.202303658 by University of Turku, Wiley Online Library on [31/05/2023]. See the Terms and Conditions (https://onlinelibrary.wiley.com/terms-and-conditions) on Wiley Online Library for rules of use; OA articles are governed by the applicable Creative Commons License

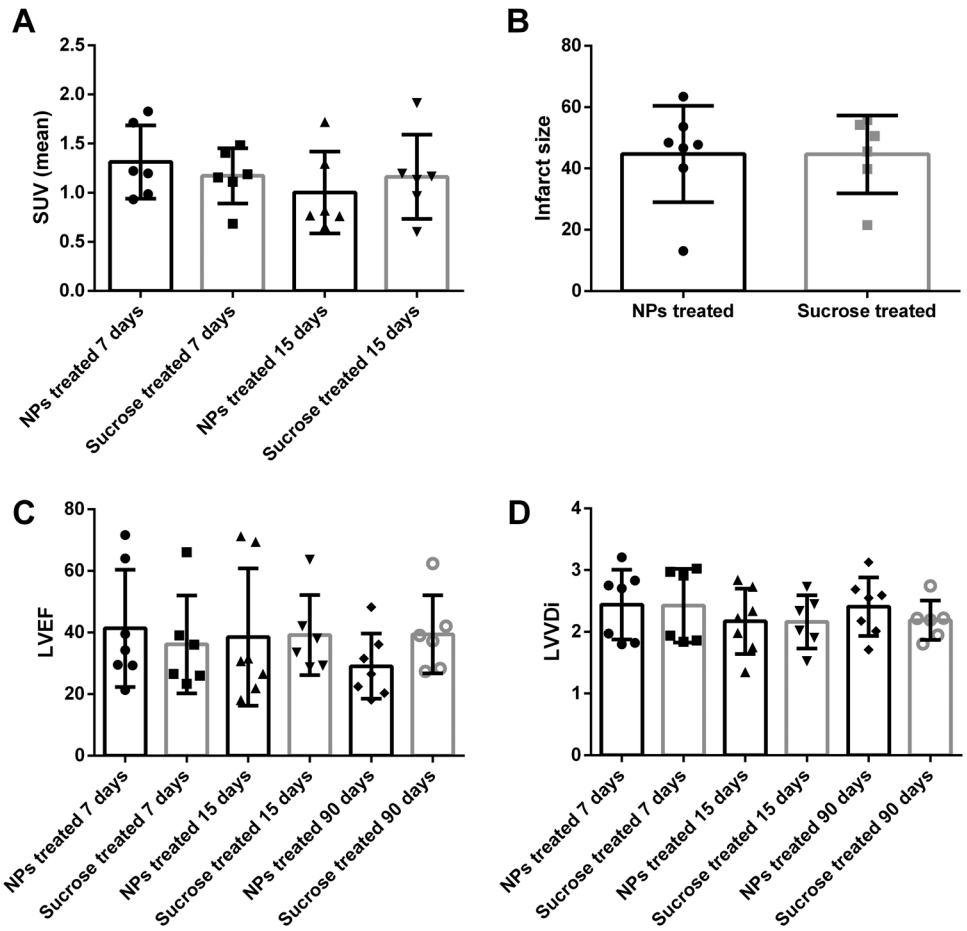

Figure 8. In vivo PET studies and evaluation of cardiac function in infarcted animals. A) The recruitment of inflammatory cells to the infarcted heart after 7- and 15-days post-MI was evaluated by following the accumulation of ^{18}F-FOL in animals treated either with Putre-AcDEX-PEG-TT1-ANP NPs or isotonic sucrose. B) The infarct size was evaluated by calculating the volumetric percentage of the affected area from H&E stainings. C) Cardiac function was evaluated by measuring the left ventricle ejection fraction (LVEF), and (D) left ventricle diastolic volume index (LVVDi). Results are presented as standardized uptake value (SUV), percentage of infarcted heart, LVEF and LVVDi ± S.D. ($n = 3$ biological replicates in which each time three technical replicates have been used). An unpaired two-tailed Student's *t*-test was used for the statistical analysis. The significance level was set at probability $^{*}p < 0.05$ for the different comparisons.

(H&E) staining of heart sections obtained from animals sacrificed after the 90 days. Infarct size measurements (Figures 8B; Figure S14B, Supporting Information) were not statistically significant different between animals injected with the NPs and isotonic sucrose, indicating that treatment with NPs was not sufficient to reduce the size of the infarct damage in the heart. This lack of efficacy was also reflected by the lack of differences in left ventricle ejection fraction (LVEF) (Figure 8C) and left ventricle diastolic volume indexed (LVDDi) (Figure 8D), which were obtained by echocardiography (related images can be found in Figure S15, Supporting Information). Sucrose and NPs-treated SHAM animals also did not show statistically significant difference in cardiac function (Figure S16, supporting Information), demonstrating in this case that NPs are not inducing any acute toxicity in injected animals. No significant differences were recorded also between the different time-point measurements.

Overall, albeit the in vivo studies did not show a therapeutic effect of the nanosystem developed here, we demonstrated that the Putre-AcDEX-PEG-TT1-ANP NPs did not induce any acute toxicity in treated animals nor modify their immunological profile. Quantification of the NPs accumulating in the heart would be useful to exclude that the lack of therapeutic efficacy was because of too low amount of NPs reaching the heart NPs. Also, modification of treatment regime by adopting different treatment schedules and analytic methods could give better insights on the actions of these NPs in vivo.

3. Conclusion

In this work, dual conjugated ANP-peptide NPs were produced to improve the heart homing properties of ANP by taking advantage of the recruitment of inflammatory cells in the infarcted tissue. For this purpose, lin-TT1 was co-conjugated onto the surface of the NPs, enhancing the NP ability to hitchhike on M2–like macrophages in vivo. This approach resulted in improved NP accumulation in the infarcted hearts at 7 days post-MI. In comparison with NPs conjugated with only ANP, NPs modified with both peptides

 © 2023 The Authors. Advanced Functional Materials published by Wiley-VCH GmbH

demonstrated superior accumulation in the heart, showing that hitchhiking on inflammatory cells improves the heart targeting of ANP. Immunoprofiling of spleens and blood showed that the NP were safe after injection in the animals and did not have acute toxic effects on immune cells. Moreover, the encapsulation of two small hydrophobic compounds, CHIR and SB, resulted in a 4-fold increase of BrdU incorporating primary CMs in vitro compared to control cells, as well as an increase on β-catenin expression in both nucleus and cytoplasm, demonstrating the potential of the drug delivered compounds in stimulating cell cycle re-entry in non-dividing CMs. The NPs also showed anti-inflammatory properties due to both the encapsulated drugs and the ANP. Pilot in vivo studies did not demonstrate an in vivo therapeutic effect of the developed NPs, however they showed that the nanosystem did not lead to acute toxicity in injected animals. Overall, this nanosystem offers a platform for therapeutic drug delivery and imaging of the infarcted heart, but further investigations are needed to better evaluate the possible therapeutic effects of the system and long-term safety profile.

4. Experimental Section

Preparation of Putre-AcDEX NPs, Surface Modifications, and Physicochemical Characterization: All polymer synthesis, NPs preparation, NPs surface modification and physico-chemical characterization protocols, were described in the Supporting Information.

Cell Studies: All protocols used for cell isolation, culture, and differentiation, are described in the Supporting Information.

In Vitro Biocompatibility: The protocols used for these studies were described in detail in the Supporting Information.

Quantitative Cell-NPs Interaction Studies on Primary Rat Cardiac Cells and Qualitative Uptake Studies: The methods used for these studies were described in detail in the Supporting Information.

Determination of cell proliferation: BrdU, β-catenin and phospho-MAPKAPK2 Immunostainings: Details and methods used for these studies were described in the Supporting Information.

Evaluation of the Phenotype Change in Murine M1– and M2–like Macrophages Treated with the NPs: Murine M1– and M2–like macrophages were differentiated from precursor cells isolated from the bone marrow of mice as described in the Supporting Information. For the studies on the phenotype change upon treatment with NPs, MØ macrophages were seeded on 12-well plates at a density of 3×10^5 cells per well and treated with different cytokines for 48 h to obtain M1– and M2–like macrophages. After 48 h, cells were treated with different NPs suspensions at a concentration of 50 µg mL^{-1} for 30, 60 or 120 min. After the different time-points, cells were detached as described in the Supporting Information file and the cells were blocked with 1% (w/v) bovine serum albumin (BSA) for 10 min. After blocking, cells were incubated for 20 min in the dark at +4 °C with a cocktail of antibodies constituted by Allophycocyanin (APC)–CD206 (BioLegend, USA) and Peridinin chlorophyll protein(PerCP)-Cyanine5.5-CD86 (BioLegend, USA). Fluorescence was detected by a BD Accuri C6 Plus (BD, USA) flow cytometer, and the data analysis was performed with FlowJo software (Tree Star, Inc., USA). Cells were gated according to Scheme S1 (Supporting Information).

Experimental Model of Myocardial Infarction (MI): The national Project Authorization Board in Finland approved the animal studies (license number ESAVI/43 134/2019). The study was carried out in compliance with the European Union directive 2010/EU/63 on the protection of animals used for scientific purposes.

MI was induced in male Sprague-Dawley rats (6-8 weeks old) by permanent ligation of the left anterior descending (or LAD) coronary artery as described previously.[59–61] The sham operation consisted of the same protocols except for the ligation of the coronary artery.

During nanoparticle injections and all imaging studies, rats were anesthetized with isoflurane (4-5% for induction and 1.5-2% for maintenance) and body temperature was maintained using a heating pad. MIs were further confirmed by H&E stainings, which were scanned with a digital slide scanner (Pannoramic 250 Flash, 3DHistech Ltd., Budapest, Hungary).

Ex Vivo Biodistribution Studies: The biodistribution of the NPs was studied at 3 days (n = 5 for each group) or 7 days (n = 5 for each group) after coronary ligation or at 3 days (n = 5 for each group) or 7 days (n = 5 for each group) after the sham operation. The rats were divided into four groups: isotonic sucrose; Putre-AcDEX-PEG NPs; Putre-AcDEX-PEG-ANP NPs; and Putre-AcDEX-PEG-TT1-ANP NPs. Animals were kept under isoflurane anesthesia (Attane Vet., ScanVet Animal Health, Finland) in air carrier at 0.4-0.6 L min^{-1} during sucrose or NPs administration. The dose of NPs administrated for each group was 2 mg. The intravenous injections were given in a volume of ≈100 µL via tail vein, followed by a flush of 0.1 mL of sterile 0.9% NaCl. One-hour post-injection, animals were sacrificed, and different organs were collected. For the study of ex vivo NPs' biodistribution hearts, livers, and spleens were collected and sliced into 8 and 20 µm sections. Liver and spleen sections were fixed with 4% paraformaldehyde (PFA) and stained with DAPI. Hearts sections were blocked with 1% BSA for 1 h after fixation and then stained with anti-CD86 (1:200, from BioRad, MCA2874GA) and anti-CD163 (1:200, from Invitrogen, PA5-78961) primary antibodies overnight at +4 °C. After overnight incubation, sections were washed 3 times for 5 min with PBS and incubated with secondary antibodies (Goat anti-mouse IgG H+L Alexa-546 (1:250, Life technologies A-11030); donkey anti-rabbit IgG H+L Alexa-647 (1:250, A-31573, Life technologies)) and DAPI (1:250, Vector Laboratories) for 1 h. Sections were washed again 3 × 5 min with PBS and slides were mounted with a non-hardening mounting media. Slides were imaged using a 63× water objective in a Leica TCS SP8 STED 3× CW 3D inverted microscope (Leica Microsystems, Germany) and images were processed with Leica AS software (Leica Microsystems, Germany) to check the presence of NPs in the different organs.

Immunoprofiling Studies: For each experimental group of the in vivo studies, liver, and spleen sections were derived from only two animals out of five. The other three animals were sacrificed and their spleens and livers were collected to study the immunoprofile of the animal upon NPs injection. Spleens were smashed onto 70 µm strainers. White cells from blood were instead separated by Ficoll-Paque (1.077 g mL^{-1} density) gradients according to the manufacturer's instructions (GE Healthcare Bio-sciences, Piscataway, NJ). White cells derived from blood and cells suspensions derived from spleens, were then blocked with 1% (v/v) of BSA for 10 min. After that, they were incubated with a cocktail of antibodies for 20 min, at +4 °C in the dark, to study the population of macrophages and T cells: APC anti-rat CD3, Phycoerythrin (PE) anti-rat CD8, and PerCP anti-rat CD4 (all from BioLegend) were used to study the T-cell population; PerCP anti-rat CD11b, AlexaFluor647 anti-rat CD86 and PE anti-rat CD163 (the first two from BioLegend and the last one from Novus Biologicals) were used to study the macrophage population. Stained cell suspensions were then washed with PBS and flow cytometry analysis was performed using a BD Accuri 6 plus (BD Biosciences) and analyzed by FlowJo software (Tree Star, Ashland, OR, USA). Cells were gated as shown in the Scheme S2 (Supporting Information).

PET/CT Studies and Evaluation of the Cardiac Function by Echocardiography: The rats underwent the PET scans with a glucose analog ^{18}F-FDG for identification of the myocardium on day 6 after MI and with ^{18}F-FOL for studying expression of folate receptor β, a marker of activated macrophages, on 7 and days 15 after MI. A computed tomography (CT) scan was performed before each PET scan for attenuation correction.

Protocols for PET/CT and image analysis were described earlier.[60–62] Briefly, the rats received standard rat food and tap water ad libitum. On average, 35 ± 5.5 MBq of ^{18}F-FDG was injected intravenously via the tail vein and the animals were scanned using a small-animal PET/CT scanner (Inveon Multimodality, Siemens Medical Solutions, Knoxville, TN, USA) for 10 min starting at 20 min after the injection. In turn, 50 ± 4.5 MBq of ^{18}F-FOL was injected intravenously via the tail vein and the animals were scanned for 20 min starting at 20 min after the injection. The ^{18}F-FOL was synthesized as previously described.[62] PET images were reconstructed

© 2023 The Authors. Advanced Functional Materials published by Wiley-VCH GmbH

16163028, 0, Downloaded from https://onlinelibrary.wiley.com/doi/10.1002/adfm.202303658 by University of Turku, Wiley Online Library on [31/05/2023]. See the Terms and Conditions (https://onlinelibrary.wiley.com/terms-and-conditions) on Wiley Online Library for rules of use; OA articles are governed by the applicable Creative Commons License

using 2 iterations with 3-dimensional ordered-subset expectations maximization (OSEM3D) and 18 maximum a posteriori (MAP) iterations algorithms.

PET images using Carimas v.2.10 software (Turku PET Centre, Turku, Finland) were analyzed. ^{18}F-FDG and ^{18}F-FOL PET images were manually superimposed. Based on myocardial contours visible in ^{18}F-FDG images, regions of interest (ROIs) were drawn in the infarcted region (defect in ^{18}F-FDG uptake) and in the remote, non-infarcted myocardium in the inferior septum to measure myocardial ^{18}F-FOL uptake 20–40 min after injection. In sham-operated rats, ROIs were drawn in myocardial regions matching those in the rats with MI. The uptake of ^{18}F-FOL in each ROI was expressed as the mean SUV calculated from the mean radioactivity concentrations (Bq/mL) normalized for injected radioactivity dose and animal weight.

Echocardiography was performed on day 7, 15, and 90 after MI using a dedicated small animal Doppler ultrasound device (Vevo 2100, VisualSonics, Inc., Toronto, ON, Canada) and a linear 13–24 MHz (MS250) transducer as previously described.[61] The left LVVDi and EF were measured by planimetry in long axis 2D images.

After the echocardiography at 90 days post-MI, the rats were euthanized, and their left ventricles were excised. The left ventricle was frozen in dry ice-cooled isopentane and cut into 8 and 20 µm sections along the short axis at 1 mm intervals. The 20-µm sections were stained with H&E, and scanned with a digital slide scanner (Pannoramic P1000, 3DHistech Ltd., Budapest, Hungary) to determine MI size as the percentage of scar of the endocardial perimeter as previously described.[59–61] MI was defined as a scar >4% of the endocardial perimeter.

Supporting Information

Supporting Information is available from the Wiley Online Library or from the author.

Acknowledgements

G.T. acknowledged the financial support of the Doctoral Programmes in Health Sciences for a short-term employment positions for dissertation completing in 2022, the Paavo Nurmi Foundation, the Finnish Cultural Foundation, and the Orion Research Foundation. V.B. acknowledged the University of Helsinki Research Funds for three-years PhD position. Prof. H.R. acknowledged the financial support from the Sigrid Jusélius Foundation and the Finnish Foundation of Cardiovascular Research. V.T. acknowledged financial support from the Academy of Finland (grant no. 321564, 1328909) and the Finnish Foundation for Cardiovascular Research. T.T. acknowledged the Estonian Research Council (TT, grants PRG230, PRG1788, and EAG79), and EuronanomedII projects ECM-CART and iNanoGun (TT). A.R. acknowledged the financial support from the Jane and Aatos Erkko Foundation and the Sigrid Jusélius Foundation. A.S. acknowledged the financial support from the Academy of Finland and Finnish Foundation for Cardiovascular Research, and fees for consultancy or lectures from Abbott, Astra Zeneca, Bayer, Novartis, and Pfizer. Prof. H.A. Santos acknowledged financial support from the Sigrid Jusélius Foundation, the Academy of Finland (grant no. 331151) and the UMCG Research Funds. The authors also acknowledged the following core facilities funded by Biocenter Finland: Electron Microscopy Unity of the University for providing the facilities for TEM imaging; Flow cytometry, MST and Biacore core facilities of the University for the flow cytometer; the Light Microscopy Unit of the Institute of Biotechnology for the confocal microscope; and the Biomedicum Imaging Unit for the high-content imaging platform. Annika Korvenpää was thanked by the authors for help with human stem cell culture and differentiation. The authors further acknowledged the technical help of the following people during the in vivo studies: Aake Honkaniemi, Erika Atencio Herre (Turku PET Centre), Erica Nyman, and Marja-Riitta Kajaala (The University of Turku Histocore facility).

Conflict of Interest

Dr. V. Balasubramanian is an employee at Bayer Oy (Finland). The other authors declare that they have no known competing financial interests or personal relationships that could have appeared to influence the work reported in this paper.

Data Availability Statement

The data that support the findings of this study are available from the corresponding author upon reasonable request.

Keywords

cardiac regeneration, heart targeting nanoparticles, hitchhiking effect, macrophage recruitment, positron emission tomography

Received: April 2, 2023
Revised: April 21, 2023
Published online:

[1] P. Joseph, D. Leong, M. McKee, S. S. Anand, J.-D. Schwalm, K. Teo, A. Mente, S. Yusuf, *Circ. Res.* **2017**, *121*, 677.
[2] A. Uygur, R. T. Lee, *Dev Cell* **2016**, *36*, 362.
[3] V. Talman, H. Ruskoaho, *Cell Tissue Res.* **2016**, *365*, 563.
[4] Z. Lin, W. T. Pu, *Sci. Transl. Med.* **2014**, *6*, 239rv1.
[5] A. Eulalio, M. Mano, M. D. Ferro, L. Zentilin, G. Sinagra, S. Zacchigna, M. Giacca, *Nature* **2012**, *492*, 376.
[6] J. Chen, Z.-P. Huang, H. Y. Seok, J. Ding, M. Kataoka, Z. Zhang, X. Hu, G. Wang, Z. Lin, S. Wang, W. T. Pu, R. Liao, D.-Z. Wang, *Circ. Res.* **2013**, *113*, 1557.
[7] E. R. Porrello, A. I. Mahmoud, E. Simpson, B. A. Johnson, D. Grinsfelder, D. Canseco, P. P. Mammen, B. A. Rothermel, E. N. Olson, H. A. Sadek, *Proc. Natl. Acad. Sci. USA* **2013**, *110*, 187.
[8] M. Xin, Y. Kim, L. B. Sutherland, M. Murakami, X. Qi, J. McAnally, E. R. Porrello, A. I. Mahmoud, W. Tan, J. M. Shelton, J. A. Richardson, H. A. Sadek, R. Bassel-Duby, E. N. Olson, *Proc. Natl. Acad. Sci. USA* **2013**, *110*, 13839.
[9] T. Heallen, Y. Morikawa, J. Leach, G. Tao, J. T. Willerson, R. L. Johnson, J. F. Martin, *Development* **2013**, *140*, 4683.
[10] K. Bersell, S. Arab, B. Haring, B. Kühn, *Cell.* **2009**, *138*, 257.
[11] S. Welch, D. Plank, S. Witt, B. Glascock, E. Schaefer, S. Chimenti, A. M. Andreoli, F. Limana, A. Leri, J. Kajstura, P. Anversa, M. A. Sussman, *Circ. Res.* **2002**, *90*, 641.
[12] H. Uosaki, A. Magadum, K. Seo, H. Fukushima, A. Takeuchi, Y. Nakagawa, K. W. Moyes, G. Narazaki, K. Kuwahara, M. Laflamme, S. Matsuoka, N. Nakatsuji, K. Nakao, C. Kwon, D. A. Kass, F. B. Engel, J. K. Yamashita, *Circ. Cardiovasc. Genet.* **2013**, *6*, 624.
[13] F. B. Engel, M. Schebesta, M. T. Duong, G. Lu, S. Ren, J. B. Madwed, H. Jiang, Y. Wang, M. T. Keating, *Genes Dev.* **2005**, *19*, 1175.
[14] C. L. Ventola, *P T.* **2012**, *37*, 512.
[15] S. Kargozar, M. Mozafari, *Mater. Today Proc.* **2018**, *5*, 15492.
[16] M. Shin, H.-A. Lee, M. Lee, Y. Shin, J.-J. Song, S.-W. Kang, D.-H. Nam, E. J. Jeon, M. Cho, M. Do, S. Park, M. S. Lee, J.-H. Jang, S.-W. Cho, K.-S. Kim, H. Lee, *Nat. Biomed. Eng.* **2018**, *2*, 304.
[17] M. P. A. Ferreira, S. Ranjan, S. Kinnunen, A. Correia, V. Talman, E. Mäkilä, B. Barrios-Lopez, M. Kemell, V. Balasubramanian, J. Salonen, J. Hirvonen, H. Ruskoaho, A. J. Airaksinen, H. A. Santos, *Small* **2017**, *13*, 1701276.
[18] T. Dvir, M. Bauer, A. Schroeder, J. H. Tsui, D. G. Anderson, R. Langer, R. Liao, D. S. Kohane, *Nano Lett.* **2011**, *11*, 4411.

© 2023 The Authors. Advanced Functional Materials published by Wiley-VCH GmbH

16163028, 0, Downloaded from https://onlinelibrary.wiley.com/doi/10.1002/adfm.202303658 by University of Turku, Wiley Online Library on [31/05/2023]. See the Terms and Conditions (https://onlinelibrary.wiley.com/terms-and-conditions) on Wiley Online Library for rules of use; OA articles are governed by the applicable Creative Commons License

[19] R. C. Scott, J. M. Rosano, Z. Ivanov, B. Wang, P. L.-G. Chong, A. C. Issekutz, D. L. Crabbe, M. F. Kiani, *FASEB J.* **2009**, *23*, 3361.
[20] J. S. Brenner, D. C. Pan, J. W. Myerson, O. A. Marcos-Contreras, C. H. Villa, P. Patel, H. Hekierski, S. Chatterjee, J.-Q. Tao, H. Parhiz, K. Bhamidipati, T. G. Uhler, E. D. Hood, R. Y. Kiseleva, V. S. Shuvaev, T. Shuvaeva, M. Khoshnejad, I. Johnston, J. V. Gregory, J. Lahann, T. Wang, E. Cantu, W. M. Armstead, S. Mitragotri, V. Muzykantov, *Nat. Commun.* **2018**, *9*, 2684.
[21] G. Torrieri, F. Fontana, P. Figueiredo, Z. Liu, M. P. A. Ferreira, V. Talman, J. P. Martins, M. Fusciello, K. Moslova, T. Teesalu, V. Cerullo, J. Hirvonen, H. Ruskoaho, V. Balasubramanian, H. A. Santos, *Nanoscale* **2020**, *12*, 2350.
[22] L. Paasonen, S. Sharma, G. B. Braun, V. R. Kotamraju, T. D. Y. Chung, Z.-G. She, K. N. Sugahara, M. Yliperttula, B. Wu, M. Pellecchia, E. Ruoslahti, T. Teesalu, *Chembiochem* **2016**, *17*, 570.
[23] J. Hamzah, V. R. Kotamraju, J. W. Seo, L. Agemy, V. Fogal, L. M. Mahakian, D. Peters, L. Roth, M. K. J. Gagnon, K. W. Ferrara, E. Ruoslahti, *Proc. Natl. Acad. Sci. USA* **2011**, *108*, 7154.
[24] V. Fogal, L. Zhang, S. Krajewski, E. Ruoslahti, *Cancer Res.* **2008**, *68*, 7210.
[25] M. Nahrendorf, F. K. Swirski, *Circ. Res.* **2013**, *112*, 1624.
[26] M. Nahrendorf, F. K. Swirski, E. Aikawa, L. Stangenberg, T. Wurdinger, J.-L. Figueiredo, P. Libby, R. Weissleder, M. J. Pittet, *J. Exp. Med.* **2007**, *204*, 3037.
[27] R. Stevens, L. Stevens, N. C. Price, *Biochem. Educ.* **1983**, *11*, 70.
[28] S. Pabisch, B. Feichtenschlager, G. Kickelbick, H. Peterlik, *Chem. Phys. Lett.* **2012**, *521*, 91.
[29] J. S. Suk, Q. Xu, N. Kim, J. Hanes, L. M. Ensign, *Adv. Drug Delivery Rev.* **2016**, *99*, 28.
[30] J. V. Jokerst, T. Lobovkina, R. N. Zare, S. S. Gambhir, *Nanomedicine (Lond)* **2011**, *6*, 715.
[31] A. Vonarbourg, C. Passirani, P. Saulnier, J.-P. Benoit, *Biomaterials* **2006**, *27*, 4356.
[32] H. A. Santos, J. Riikonen, J. Salonen, E. Mäkilä, T. Heikkilä, T. Laaksonen, L. Peltonen, V.-P. Lehto, J. Hirvonen, *Acta Biomater.* **2010**, *6*, 2721.
[33] E. Fröhlich, *Int J Nanomedicine* **2012**, *7*, 5577.
[34] K. N. Pandey, *Mol. Cell. Biochem.* **2002**, *230*, 61.
[35] L. Xu, S. Chen, R. C. Bergan, *Oncogene* **2006**, *25*, 2987.
[36] G. Ozhan, G. Weidinger, *Cell Regen.* **2015**, *4*, 4:3.
[37] F. B. Engel, M. Schebesta, M. T. Keating, *J. Mol. Cell. Cardiol.* **2006**, *41*, 601.
[38] Y. Fan, B. X. Ho, J. K. S. Pang, N. M. Q. Pek, J. H. Hor, S.-Y. Ng, B.-S. Soh, *Stem Cell Res Ther* **2018**, *9*, 338.
[39] M. Verheijen, M. Lienhard, Y. Schrooders, O. Clayton, R. Nudischer, S. Boerno, B. Timmermann, N. Selevsek, R. Schlapbach, H. Gmuender, S. Gotta, J. Geraedts, R. Herwig, J. Kleinjans, F. Caiment, *Sci. Rep.* **2019**, *9*, 4641.
[40] L. Wang, Y. Wang, C. Zhang, J. Li, Y. Meng, M. Dou, C. T. Noguchi, L. Di, *Arterioscler Thromb Vasc Biol* **2018**, *38*, 2103.
[41] Q. Shi, L. Cheng, Z. Liu, K. Hu, J. Ran, D. Ge, J. Fu, *Cent. Eur. J. Immunol.* **2015**, *40*, 276.
[42] A. K. Kiemer, A. M. Vollmar, *Ann. Rheum. Dis. 60 Suppl 3* **2001**, *60*, 68.
[43] L. Mezzasoma, V. N. Talesa, R. Romani, I. Bellezza, *Int. J. Mol. Sci.* **2020**, *22*, 24.
[44] S. Roy, A. K. Bag, R. K. Singh, J. E. Talmadge, S. K. Batra, K. Datta, *Front Immunol* **2017**, *8*, 1228.
[45] E. Blanco, H. Shen, M. Ferrari, *Nat. Biotechnol.* **2015**, *33*, 941.
[46] M. Cataldi, C. Vigliotti, T. Mosca, M. Cammarota, D. Capone, *Int. J. Mol. Sci.* **2017**, *18*, 1249.
[47] S. M. Moghimi, H. Hedeman, I. S. Muir, L. Illum, S. S. Davis, *Biochim Biophys Acta Gen Subj BBA-GEN SUBJECTS* **1993**, *1157*, 233.
[48] I. Santos-Zas, J. Lemarié, I. Zlatanova, M. Cachanado, J.-C. Seghezzi, H. Benamer, P. Goube, M. Vandestienne, R. Cohen, M. Ezzo, V. Duval, Y. Zhang, J.-B. Su, A. Bizé, L. Sambin, P. Bonnin, M. Branchereau, C. Heymes, C. Tanchot, J. Vilar, C. Delacroix, J.-S. Hulot, C. Cochain, P. Bruneval, N. Danchin, A. Tedgui, Z. Mallat, T. Simon, B. Ghaleb, J.-S. Silvestre, et al., *Nat. Commun.* **2021**, *12*, 1483.
[49] D. V. Ilatovskaya, C. Pitts, J. Clayton, M. Domondon, M. Troncoso, S. Pippin, K. Y. DeLeon-Pennell, *Am J Physiol Heart Circ Physiol* **2019**, *317*, H581.
[50] U. Hofmann, N. Beyersdorf, J. Weirather, A. Podolskaya, J. Bauersachs, G. Ertl, T. Kerkau, S. Frantz, *Circulation* **2012**, *125*, 1652.
[51] J. Weirather, U. D. W. Hofmann, N. Beyersdorf, G. C. Ramos, B. Vogel, A. Frey, G. Ertl, T. Kerkau, S. Frantz, *Circ. Res.* **2014**, *115*, 55.
[52] P. De Vito, *Peptides* **2014**, *58*, 108.
[53] S. Kawano, T. Kubota, Y. Monden, T. Tsutsumi, T. Inoue, N. Kawamura, H. Tsutsui, K. Sunagawa, *Am J Physiol Heart Circ Physiol* **2006**, *291*, H1337.
[54] C.-X. Huang, M.-J. Yuan, H. Huang, G. Wu, Y. Liu, S.-B. Yu, H.-T. Li, T. Wang, *Peptides.* **2009**, *30*, 2286.
[55] S. Huang, N. G. Frangogiannis, *Br. J. Pharmacol.* **2018**, *175*, 1377.
[56] J. Grune, A. J. M. Lewis, M. Yamazoe, M. Hulsmans, D. Rohde, L. Xiao, S. Zhang, C. Ott, D. M. Calcagno, Y. Zhou, K. Timm, M. Shanmuganathan, F. E. Pulous, M. J. Schloss, B. H. Foy, D. Capen, C. Vinegoni, G. R. Wojtkiewicz, Y. Iwamoto, T. Grune, D. Brown, J. Higgins, V. M. Ferreira, N. Herring, K. M. Channon, S. Neubauer, M. Shanmuganathan, V. M. Ferreira, K. M. Channon, D. E. Sosnovik, et al., *Nat. Cardiovasc. Res.* **2022**, *1*, 649.
[57] A. Müller, K. Beck, Z. Rancic, C. Müller, C. R. Fischer, T. Betzel, P. A. Kaufmann, R. Schibli, S. D. Krämer, S. M. Ametamey, *Mol Imaging* **2014**, *13*, 7290.
[58] J. M. U. Silvola, X.-G. Li, J. Virta, P. Marjamäki, H. Liljenbäck, J. P. Hytönen, M. Tarkia, V. Saunavaara, S. Hurme, S. Palani, H. Hakovirta, S. Ylä-Herttuala, P. Saukko, Q. Chen, P. S. Low, J. Knuuti, A. Saraste, A. Roivainen, *Sci. Rep.* **2018**, *8*, 9720.
[59] M. A. Pfeffer, J. M. Pfeffer, M. C. Fishbein, P. J. Fletcher, J. Spadaro, R. A. Kloner, E. Braunwald, *Circ. Res.* **1979**, *44*, 503.
[60] M. Kiugel, I. Dijkgraaf, V. Kytö, S. Helin, H. Liljenbäck, T. Saanijoki, C.-B. Yim, V. Oikonen, P. Saukko, J. Knuuti, A. Roivainen, A. Saraste, *Mol. Imaging Biol.* **2014**, *16*, 793.
[61] M. Ståhle, V. Kytö, M. Kiugel, H. Liljenbäck, O. Metsälä, M. Käkelä, X.-G. Li, V. Oikonen, P. Saukko, P. Nuutila, J. Knuuti, A. Roivainen, A. Saraste, *J. Nucl. Cardiol. Off. Publ. Am. Soc. Nucl. Cardiol.* **2020**, *27*, 2386.
[62] A. Jahandideh, S. Uotila, M. Ståhle, J. Virta, X.-G. Li, V. Kytö, P. Marjamäki, H. Liljenbäck, P. Taimen, V. Oikonen, J. Lehtonen, M. I. Mäyränpää, Q. Chen, P. S. Low, J. Knuuti, A. Roivainen, A. Saraste, *J Nucl Med* **2020**, *61*, 1643.

© 2023 The Authors. Advanced Functional Materials published by Wiley-VCH GmbH

16163028, 0, Downloaded from https://onlinelibrary.wiley.com/doi/10.1002/adfm.202303658 by University of Turku, Wiley Online Library on [31/05/2023]. See the Terms and Conditions (https://onlinelibrary.wiley.com/terms-and-conditions) on Wiley Online Library for rules of use; OA articles are governed by the applicable Creative Commons License